FISEVIER

#### Contents lists available at ScienceDirect

# Journal of Hydrology

journal homepage: www.elsevier.com/locate/jhydrol



#### Research papers

# Watershed erosion modeling using the probability of sediment connectivity in a gently rolling system



David Tyler Mahoney, James Forrest Fox\*, Nabil Al Aamery

Department of Civil Engineering, University of Kentucky, United States

#### ARTICLE INFO

This manuscript was handled by G. Syme, Editor-in-Chief

Keywords: Sediment transport Stochastic Watershed scale Disconnectivity

#### ABSTRACT

Sediment connectivity has been shown in recent years to explain how the watershed configuration controls sediment transport. However, we find no studies develop a watershed erosion modeling framework based on sediment connectivity, and few, if any, studies have quantified sediment connectivity for gently rolling systems. We develop a new predictive sediment connectivity model that relies on the intersecting probabilities for sediment supply, detachment, transport, and buffers to sediment transport, which is integrated in a watershed erosion model framework. The model predicts sediment flux temporally and spatially across a watershed using field reconnaissance results, a high-resolution digital elevation models, a hydrologic model, and shear-based erosion formulae. Model results validate the capability of the model to predict erosion pathways causing sediment connectivity. More notably, disconnectivity dominates the gently rolling watershed across all morphologic levels of the uplands, including, microtopography from low energy undulating surfaces across the landscape, swales and gullies only active in the highest events, karst sinkholes that disconnect drainage areas, and floodplains that de-couple the hillslopes from the stream corridor. Results show that sediment connectivity is predicted for about 2% or more the watershed's area 37 days of the year, with the remaining days showing yery little or no connectivity. Only 12.8 ± 0.7% of the gently rolling watershed shows sediment connectivity on the wettest day of the study year. Results also highlight the importance of urban/suburban sediment pathways in gently rolling watersheds, and dynamic and longitudinal distributions of sediment connectivity might be further investigated in future work. We suggest the method herein provides the modeler with an added tool to account for sediment transport criteria and has the potential to reduce computational costs in watershed erosion modeling.

#### 1. Introduction

Watershed erosion modeling aims to simulate sediment flux in a basin to discern impacts of sediment loss on landscape practices and sediment impacts on stream biology, reservoir water supply, and water quality (Morris and Fan, 2009; USEPA, 2004). However, quantifying watershed erosion has proven precarious due to spatially diverse landscapes that can buffer and disconnect sediment pathways (Fryirs, 2013). We argue sediment connectivity theory provides a meaningful concept to elucidate the role of the watershed configuration and advance watershed erosion modeling, especially in light of now often available high-resolution digital elevation models. Our motivation was to develop a probability-based theory of sediment connectivity that may be integrated within continuous-based watershed erosion simulations. We apply our modeling framework with the intent to gain knowledge of sediment disconnectivity in gently rolling terrains, which are understudied.

Currently, there is a need to advance watershed erosion models within the water resources community. Substantial advancement of watershed erosion modeling over the past four decades results from the intensive field data collection systems and experimental watersheds of the 1970s and 1980s, the coupled hydrologic formulae advancement of the 1980s, and the computational and geospatial data advancements of the 1990s and 2000s (Walling, 1983; Merritt et al., 2003; Mahoney, 2017). Researchers and practitioners now have watershed erosion modeling platforms that are often freely available and can be readily applied. However, current watershed models often do not explicitly account for the three-dimensional spatial complexity of the landscape and its dynamic nature when predicting erosion and routing of sediment. The advanced ability of our current computational environment allows parameterization of watershed erosion models that shifts the physical-based functions within the models away from the inputs and parameters for which the equations were originally designed. Often, the governing erosion formulae providing the basis of the watershed model

<sup>\*</sup> Corresponding author at: Department of Civil Engineering, University of Kentucky, 354G O. H. Raymond Bldg., Lexington, KY 40506-0281, United States. E-mail addresses: tyler.mahoney@uky.edu (D.T. Mahoney), james.fox@uky.edu (J.F. Fox), nabil.hussain@uky.edu (N. Al Aamery).

is one, or a few, assumed erosion processes (e.g., plot scale sheet flow). Extrapolating these processes to the entire watershed surface produces an empirically parameterized model, assuming sufficient verification data, in which the modeler produces a posterior solution space that may not reflect the sediment detachment and transport occurring across the uplands. In this case, the modeler neglects the three dimensional and temporally dynamic landscape.

Presently, we detail a promising approach to help overcome spatial complexity limitations and advance watershed erosion modeling by coupling erosion formulae with sediment connectivity using high-resolution spatial data. We argue the time is ripe to advance watershed erosion modeling by improving its spatiotemporal context for several reasons. Highly resolved topographic datasets are often freely available, making incorporation of such data into watershed platforms feasible. Also, geomorphologic field-based and geospatial-based investigation have been advanced in recent years to focus on the topic of 'sediment connectivity.'

Sediment connectivity is a contemporary term that we define similarly to Bracken et al. (2015) as the integrated detachment and transport of sediment from source to sink between geomorphic zones of a watershed. While the term is contemporary, we recognize general concern for how erosion zones are connected to the stream channel (i.e., sediment delivery) has been studied for the past 60 years (e.g., Maner and Barnes, 1953; Glymph, 1954; Schumm, 1954), if not earlier. The contemporary definition of sediment connectivity has evolved from several bodies of sediment transport and geomorphologic literature. One body of literature is research focused on the sediment delivery ratio, which was developed in the 1950s and 60s by Maner and Barnes (1953), Roehl (1962), and studied extensively thereafter. A second body of literature is the work by Schumm (1977) and researchers thereafter, which conceptually compartmentalizes zones of the watershed by their respective dominance of sediment production, transfer, and deposition. This work led to numerous studies assessing sediment source-to-channel delivery at various scales (e.g., Ferguson, 1981; Roberts and Church, 1986; Knighton, 1989; Brunsden, 1993; Harvey, 1996; Michaelides and Wainwright, 2002). The third body of literature is general connectivity theory, which is defined as the transfer of matter between two landscape compartments or throughout an entire system (Chorley and Kennedy, 1971). General connectivity theory was further developed by ecologists (e.g., Taylor et al., 1993; Pringle, 2003) until adopted by geomorphologists to describe the hydrologic connection of geomorphologic compartments.

The contemporary idea of sediment connectivity has evolved by synthesizing the above literature bodies. Contemporary sediment connectivity aims to identify the watershed's configuration and its role within the sediment continuum including the stores and sinks of sediment, the pathways of sediment detachment and transport, and the morphologic features disconnecting the pathways of sediment transport during hydrologic events (Fryirs et al., 2007; Jain and Tandon, 2010) to work towards solving the 'sediment delivery problem' (Walling, 1983). Contemporary sediment connectivity gained popularity in the earlyand mid-2000s through conceptual work from researchers such as Hooke (2003), Brierley et al. (2006), Fryirs et al. (2007), Bracken and Croke (2007) and Bracken et al. (2015), and was extended to morphological budgeting (Croke et al., 2013) and morphometric analysis (Marchamalo et al., 2016). Current application of sediment connectivity includes index-based, empirical, and process-based analyses (e.g. Borselli et al., 2008; Messenzehl et al., 2014; Liu and Fu, 2016; Masselink et al., 2016; Heckmann and Schwanghart, 2013). Sediment connectivity is implicit within empirical models such as the sediment delivery ratio, but as identified by many researchers (e.g., Walling, 1983; Bracken and Croke, 2007; Fryirs, 2013), these historic sediment models lack integration of the complex physical processes governing sediment erosion, transport, and deposition due to spatial and temporal lumping. Sediment connectivity is now recognized to be a major control on sediment budgets (Fryirs et al., 2007), but has seldom taken precedence in quantitative sediment transport models (Ambroise, 2004; De Vente et al., 2005; Heckmann and Schwanghart, 2013).

We suggest sediment connectivity's emphasis on the watershed's configuration provides a meaningful descriptive and topologic concept for integrating within watershed erosion modeling. Numerous features of sediment connectivity, including its emphasis on field assessment and geospatial modeling, are attractive for advancing watershed erosion modeling. Field assessment of the watershed's morphology provides the foundation of sediment connectivity theory and allows identification of features that may disconnect sediment pathways lacking inclusion in watershed modeling frameworks. For example, field assessments identify sediment transport buffers such as long flat floodplains that laterally disconnect hillslopes to the stream corridor (Fryirs. 2013). Spatially explicit modeling of the watershed via sediment connectivity models has the potential to reflect the actual three-dimensional landscape to elucidate zones of active erosion and concentrated pathways of sediment transport (Cavalli et al., 2013). Thereafter, researchers may apply erosion formulae typical of watershed models to active erosion zones and active contributing area of the watershed (Ambroise, 2004), rather than extrapolating and calibrating formulae beyond their physical-basis across the entire landscape.

We commend the pioneering and recent efforts of scientists to advance the theory and application of sediment connectivity (e.g., Fryirs et al., 2007; Borselli et al., 2008; Cavalli et al., 2013; Fryirs, 2013; Bracken et al., 2015; Souza et al., 2016), which in turn provides a promising basis for improving watershed erosion models. However, we highlight several features of sediment connectivity theory requiring further development to allow integration with continuous-based watershed erosion model simulations. First, previous sediment connectivity modeling has focused on one or a few factors controlling sediment transport in a watershed such as Fryirs et al. (2007) who focused on sediment "dis" connectivity and Borselli et al. (2008), who focused on upstream and downstream sediment transport. A recent perspective article emphasizes the need to consider the many hydrologic and non-hydrologic factors controlling sediment connectivity across a watershed (Bracken et al., 2015). Therefore, our approach aims to extend sediment connectivity theory by developing a probabilistic framework that accounts for hydrologic and non-hydrologic supply, detachment, transport, and disconnectivity features. Second, sediment connectivity is dynamic by its nature and varies temporally, yet most models of sediment connectivity are static, emphasizing physical-connections in the landscape and do not capture dynamic features such as varying soil moisture conditions (Ambroise, 2004; Lexartza-Artza and Wainwright, 2009; Fryirs, 2013). Therefore, our approach aims to couple hydrologic connectivity within the watershed modeling framework to help elucidate the dynamic nature of sediment connectivity. Third, we remind the reader that sediment connectivity alone does not provide erosive flux prediction (Bracken et al., 2015), and therefore we couple their sediment connectivity theory with erosive formulae within the watershed modeling framework.

As a second contribution, we advance knowledge of sediment disconnectivity for 'gently rolling' watersheds. Most slopes of our study watershed are 'gentle' or 'undulating' although the steeper sections of complex hillslopes are classified as 'rolling' in our system (Sims et al., 1968, pp. 58; USDA, 2017 pp. 44). To highlight this idea, we use the term gently rolling watershed, which has been used previously concerning watersheds with similar terrain where fine sediment deposition occurs (e.g., Morris and Fan, 2009) and used extensively to describe our study region (McGrain, 1983 and citations thereafter). The upland morphology of gently rolling watersheds includes relatively stable land surfaces and ephemeral pathways (Jarrit and Lawrence, 2007; Ford and Fox, 2014). Mild gradients and fertile soils of gently rolling watersheds foster agricultural and suburban land uses, which in turn further stabilizes the morphology of the sediment pathways and floodplains. Previous studies investigating sediment disconnectivity emphasize moderate and steep gradient systems (e.g., Fryirs et al., 2007; Borselli

et al., 2008), and gently rolling watersheds have been understudied.

The objective of the present research was twofold and includes (i) developing a watershed erosion model grounded in probability theory for sediment connectivity and (ii) investigating sediment connectivity and erosion within a gently rolling watershed. We present a probabilistic-based development of sediment connectivity that is general to the governing factors controlling sediment transport but can be tailored and parameterized for a watershed-specific configuration. We include the concept of dynamic connectivity of sediment transport by integrating hydrologic connectivity within a continuous-based model simulation. We use probability theory to develop a predictive model reliant upon the intersecting probabilities for sediment supply. detachment, transport, and the absence of buffers. The model predicts sediment flux temporally and spatially across the watershed using highresolution geospatial data, field reconnaissance, external modeling of hydrologic connectivity, and erosion formulae. We apply the model to a gently rolling watershed to fulfill our second objective.

#### 2. Modeling framework and formulation

The watershed erosion modeling framework includes geospatial, field assessment and meteorological inputs that lead to three stages of model simulation to produce spatially and temporally explicit sediment connectivity and flux outputs (see Fig. 1). High-resolution geospatial data reflect the actual three-dimensional landscape of the watershed. Inputs from field assessment identify features that may connect and disconnect sediment pathways across the watershed. Continuous precipitation and weather data provide information leading to the dynamic nature of the watershed's connectivity.

The first stage of modeling assists with simulating dynamic connectivity by integrating hydrologic connectivity within a continuous-based model simulation. For this stage, we prescribe use of an off-the-shelf hydrologic model providing continuous simulation of soil moisture conditions and runoff depth across the watershed.

The second stage of modeling simulates the probability of sediment connectivity (see Fig. 2) to estimate pathways and buffers impacting the delivery of sediment from the uplands to the stream corridor, as a precursor to erosion rates and routing in stage three. We express the intersecting probabilities of sediment supply, detachment, transport, and the absence of buffers to produce the probability of sediment connectivity. In Fig. 2, we specify the union of both hydrologic and non-hydrologic processes. Mathematically, we express the probability of sediment connectivity, P(C), as

$$P(C) = P(S) \cap P(D_H \cup D_{NH}) \cap P(T_H \cup T_{NH}) \cap \{1 - P(B)\}$$
(1)

where S denotes supply,  $D_H$  is hydrologic detachment,  $D_{NH}$  is non-hydrologic detachment,  $T_H$  is hydrologic transport,  $T_{NH}$  is non-hydrologic transport, and B is buffers. The intersections and unions of probabilities via their multiplicative and summation definitions becomes

$$P(C) = \{P(S)\} \times \{P(D_H) + P(D_{NH}) - P(D_H)P(D_{NH})\} \times \{P(T_H) + P(T_{NH}) - P(T_H)P(T_{NH})\} \times \{1 - P(B)\}$$
(2)

The probability of sediment connectivity can be calculated when each process-associated probability is known or can be estimated. In the present study, we take a Boolean approach to Eq. (2) by modeling each geospatial grid cell represented across the landscape as having a probability of zero or one, and then integration provides the watershed's net probability of sediment connectivity. We keep Eq. (2) as general for the moment highlighting that future work could adopt a fuzzy or Bayesian approach to the probabilities of each spatial cell.

Several features of Eq. (2) require some elaboration as to their background and justification. First, we adopt a probabilistic definition of sediment connectivity because we recognize the stochastic nature of sediment transport across a heterogeneous landscape. Probability theory has long been a suitable approach to the sediment transport

problem given the non-uniformity of sediment size distributions, the stochastic nature of turbulence, and the heterogeneity of landscapes (see examples of such studies in Table 1). Concerning sediment connectivity, the probability approach is attractive because of its multiplicative ability to account for the many processes required for transport. Our approach reflects the ideas of Borselli et al. (2008), who defines the probability of connectivity as the probability that the landscape can transport sediment laterally and longitudinally in the fluvial network. Second, the probability of sediment connectivity model reflects the necessity for co-occurrence of sediment supply, detachment, and transport conditions, as these processes are well known to potentially limit transport (Leopold et al., 1964). Third, the model accepts the dynamic nature of the sediment transport controls (e.g., Jeneso et al., 2009) and thus couples with the stage one modeling. Fourth, we include both non-hydrologic connectivity, i.e., connectivity caused by non-fluvial processes, and hydrologic connectivity given the recent realization of non-hydrologic prevalence (eolian transport, landslides) in some systems at some time scales (see theory by Bracken et al., 2015). Fifth, we explicitly include the concept of disconnectivity via morphologic features and anthropogenic obstacles given the recent realization that buffers can create sediment disconnectivity (Fryirs et al., 2007; Fryirs, 2013).

The probability model in Eq. (2) may be applied for an entire watershed by using spatially explicit information across the landscape and thus reflects a distributed watershed modeling framework. The output may be used to map erosion prone features and disconnected regions. The output has specific utility in watershed erosion modeling because the probability of sediment connectivity for a hydrologic event is distributed spatially and can be integrated to estimate the active watershed area for sediment transport.

The third stage of modeling simulates erosion formulae for connected features and is tailored to the specific erosion processes known to exist in a watershed. Parameterization of the erosion formulae will vary depending on the timescale of intent, the spatial scale reflecting the connected feature, and the dominant sediment transport processes distributed across the upland landscape (e.g., mass wasting, fluvial erosion, eolian transport). Outputs include both distributed soil loss and net sediment transport results. We intend that the model may be verified *via* practical qualitative data of erosional features as well as quantitative data such that the model may be useful as a predictive tool in watershed studies.

# 3. Modeling application

# 3.1. Study site

We applied the model to the Upper South Elkhorn watershed (65.1 km²), located in the Inner Bluegrass physiographic region of Kentucky USA (see Fig. 3). The watershed has mixed land uses, consisting of primarily agricultural lands (55%) and urban areas (45%) (Fry et al., 2011). The watershed was chosen for model application because (i) past studies conducted in the watershed provide data results for calibration of modeling (Davis, 2008; Fox et al., 2010; Russo, 2009; Ford, 2011; Russo and Fox, 2012; Ford, 2014); (ii) on-going data collection is conducted by the University of Kentucky and the United States Geological Survey (USGS); and (iii) the proximity of the watershed to the University of Kentucky.

Headwaters of the South Elkhorn Creek originate in southwestern Lexington, Kentucky, within urban areas and the middle and lower watershed extends into agricultural pastureland. Gently rolling hills and relatively mild slopes characterize the land surface. The stream channel is bedrock-controlled with fine sediment deposits. Silt loams primarily make up the South Elkhorn watershed's soil cover. Upland erosion occurs primarily through rill erosion and ephemeral gully erosion, while diffusional erosion processes (i.e., sheet and interrill erosion) are a minor contribution to the overall sediment flux (Gumbert,

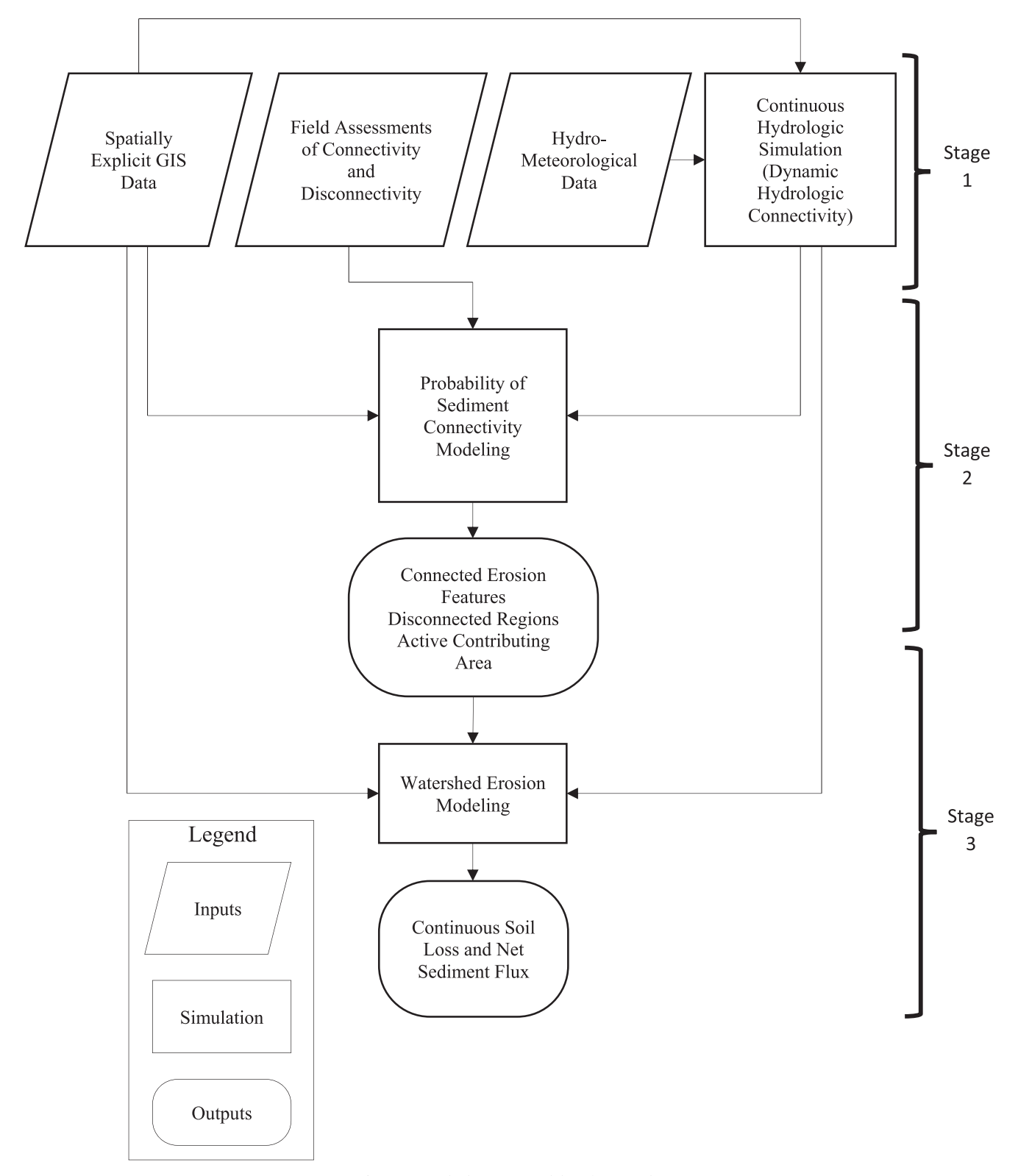


Fig. 1. Watershed erosion modeling framework.

2017; Smallwood, 2017). Livestock and construction sites in the uplands exacerbate the detachment rates of sediment particles through the removal of protective vegetation and exposure to fluvial shear stresses (Evans, 2017). The Upper South Elkhorn watershed is also characterized by long, flat floodplains adjacent to the stream network. Air temperature ranges between, on average, 0.5 °C in January to 24.5 °C in July. The average yearly rainfall for this region is 1148 mm. The

climate is classified as humid subtropical (Ulack et al., 1998).

The Inner Bluegrass Region of Kentucky USA is well-recognized as exhibiting terrain with high karst potential (Thrailkill, 1974; Thrailkill et al., 1991; Phillips, 2015), with the land surface showing depressions and sinkholes leading to springsheds. Based on analyses of geospatial data files and results published by Taylor and Nelson (2008) and the Kentucky Geological Survey (KGS, 2017), the sub-region of the South

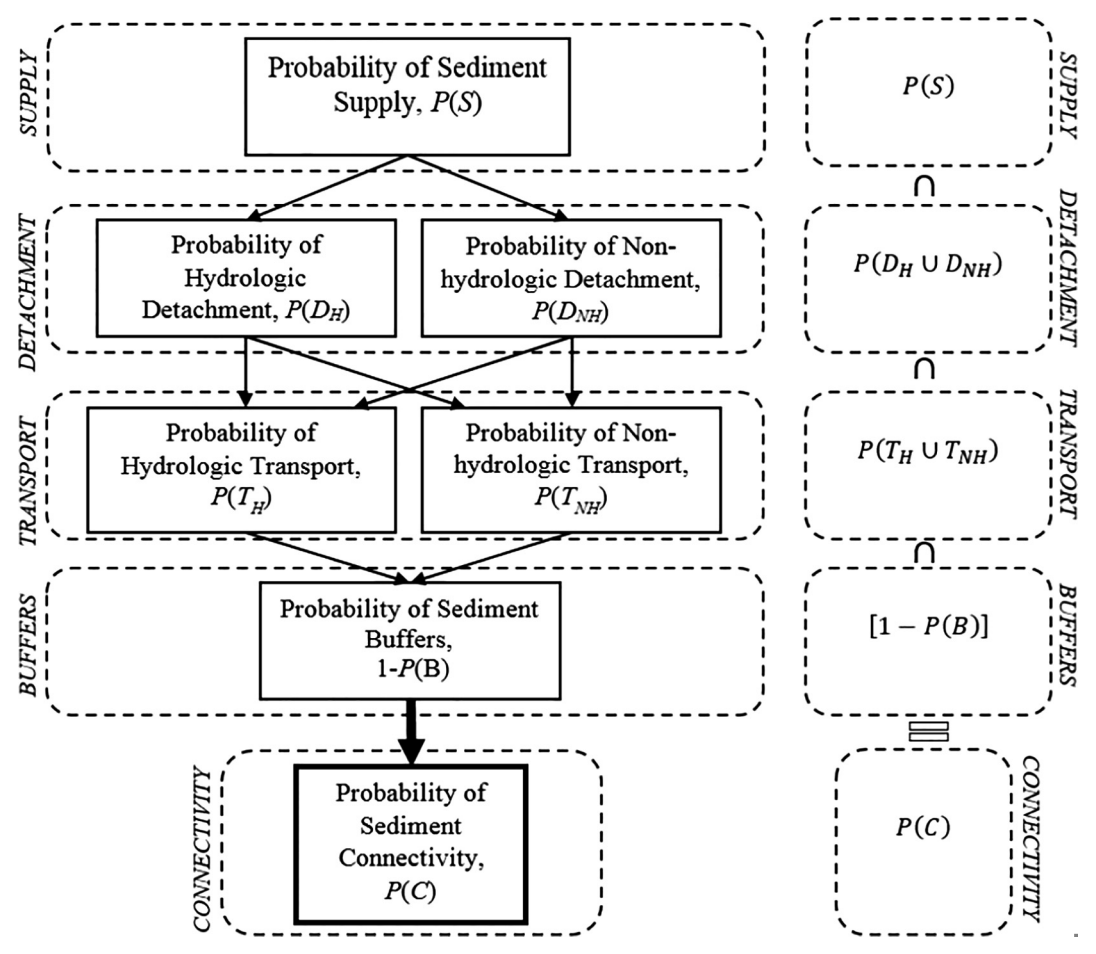


Fig. 2. Probability-based model of sediment connectivity.

**Table 1** Probability theory in sediment transport studies.

Sediment Transport Topics that Adopt Probability Theory	Examples of Published Studies				
Incipient motion and entrainment	Gessler, 1970; Grass, 1970; He and Han, 1982; Torri et al., 1990; Hsu and Holly, 1992; Cheng and Chiew, 1998; Lisle et al., 1998; Papanicolaou et al., 2002; Wu and Chou, 2003				
Sediment deposition and residence time	Dietrich et al., 1982; Celik and Rodi, 1988; Lumborg, 2004; Malmon et al., 2003; Pan and Huang, 2010				
Erosion modeling inputs and parameters	Wright and Webster, 1991; Govindaraju and Kavvas, 1992; Lewis et al., 1994; Quinton, 1997; Lisle et al., 1998; Haschenburger, 1999; Govindaraju, 1998; Foster and Fell, 2000; Baban and Yusof, 2001; Robichaud et al., 2007				
Sediment export and flux	Burns, 1979; Verhoff et al., 1979; Tazioli, 1981; Borselli et al., 2008				

Elkhorn Watershed is immature karst terrain (e.g., termed channelrich/karst-poor, Phillips et al., 2004) relative to neighboring and nearby watersheds in the Inner Bluegrass. For example, the karst-impacted drainage area of the South Elkhorn Watershed is very low ( $\sim$ 13% of the watershed drainage area, see Table 2) relative to other watersheds in the Inner Bluegrass Region (e.g., nearby watersheds show karst-impacted drainage areas ranging from 26 to 99%, see Table 2). The result is highly consistent with past morphologic research in the Inner Bluegrass karst region where the landscape is organized into discrete local zones dominated by either karst or fluvial features, to the near-exclusion of the other (Phillips et al., 2004). Dye traces performed in the South Elkhorn Watershed have shown that existing sinkhole to spring flow pathways follow the same general pathways as topographic flowlines (Currens et al., 2002). Therefore, we assume sediment pirated by sinkholes likely does not leave the watershed's topographic boundary. Nevertheless, we realized the potential importance of the karst sinkhole to impart sediment disconnectivity. Hence, we explicitly include the role of the karst terrain in watershed sediment connectivity

modeling.

# 3.2. Field Assessment, geospatial data and hydrologic data

A field assessment and geospatial analyses method was designed and carried out to identify sediment processes (e.g., sheet, rill, and gully erosion, instream sediment storage, channel morphology) and sediment disconnectivity. The field method combined published methods to visually assess sediment in watersheds and streams, including region-specific methods (NRCS, 2009; Rosgen, 2001; USEPA, 1999; Fryirs et al., 2007; Third Rock Consultants, 2016). Geospatial analyses of high-resolution digital elevation models (DEMs) and orthophotos complimented the field work and were used to map karst sinkholes in the basin.

Before field visits, we created maps in *ArcGIS* (version 10.4.1) showing the stream corridor, surrounding land cover, and tributaries. We discretized reaches into sub-reaches and spatially identified features for field inspection.

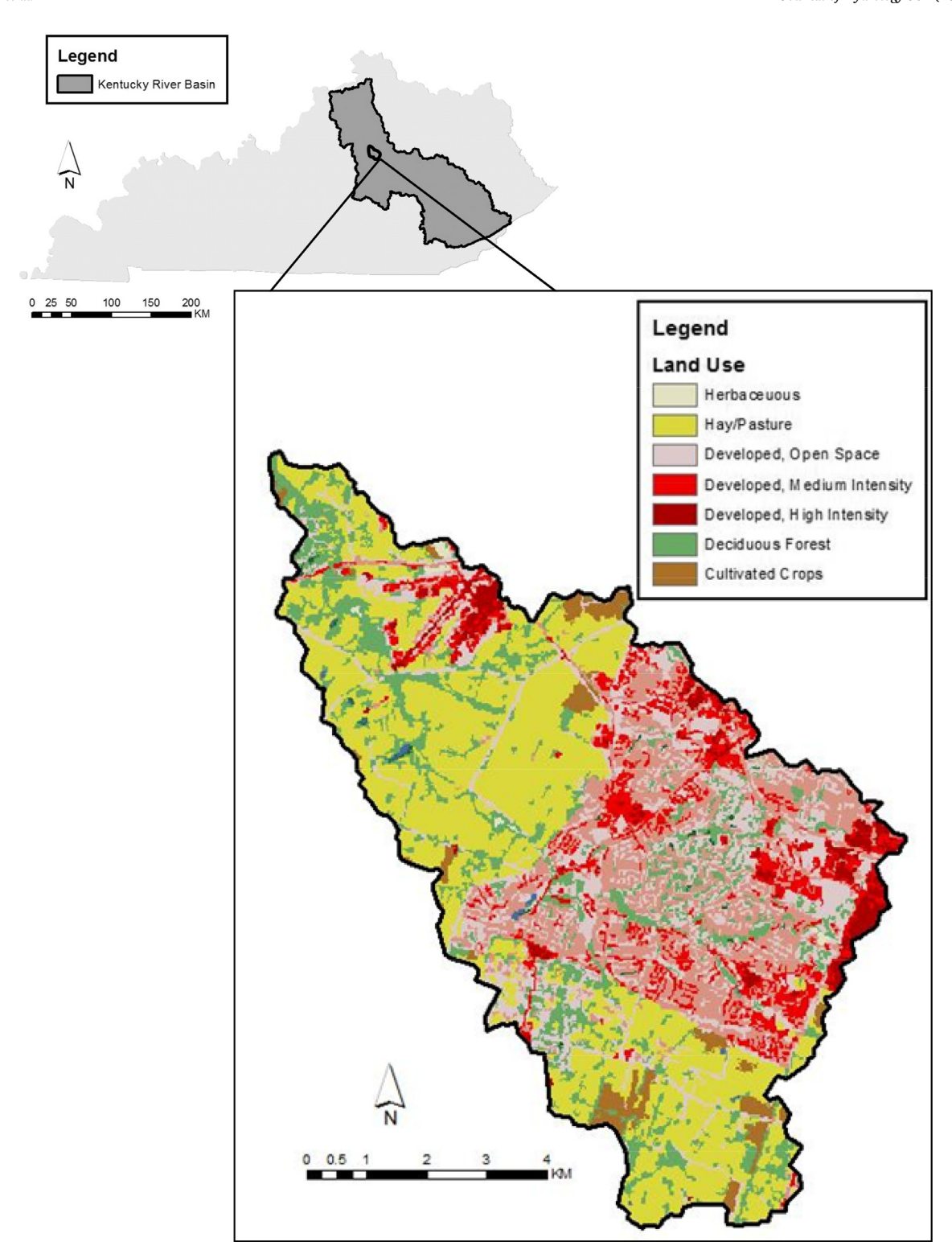


Fig. 3. Study watershed location within the Kentucky River Basin, USA and land use.

In the field, we assessed connectivity of streambanks and flood-plains, the streambed, upland hillslopes, and tributaries. We observed the density of vegetation surrounding the stream, the structure of the banks, and human infrastructure potentially influencing sediment transport. We estimated channel bathymetry, morphology, and the type and depth of sediment stored in the streambed. We assessed hillslope conditions through identification of the type of land use, evidence of historic upland erosion, and upland human interferences that may accelerate sediment transport *via* visual observations from within the

stream network coupled with orthophotograph assessment. We walked tributaries and noted bank angles, heights, bed material, erosional hotspots, and upstream land cover. We geolocated photographs of (dis) connectivity within the watershed including check dams, bedrock outcrops, point bars, depositional zones, armoring zones, connected hillslopes, floodplains, in-stream features (riffles, runs, and pools) as well as upland features (human or livestock interference). To assess long-term connectivity, we coupled this method with the following procedures: (1) we inferred evidence of strongly connected sediment

Journal of Hydrology 561 (2018) 862-883

**Table 2**Karst sinkhole drainage of the South Elkhorn and other neighboring Inner Bluegrass watersheds.

*HUC 14 Watershed	Watershed Area (km²)	Sinkhole Drainage Area (km²)	Percent Karst
Upper South Elkhorn Watershed	65.1	8.3	12.8%
Cane Run Watershed	118.0	75.2	63.8%
Sinking Creek Watershed	18.7	18.5	98.9%
Steels Run Watershed	18.2	4.8	26.3%
Lee Branch	61.4	27.3	44.5%

\*HUC 14 delineations are consistent with the revised USGS Watershed Boundary Dataset and the Hydrologic Unit Code (HUC) 14 description is consistent with Seaber et al. (1987).

transport pathways in the field by mapping erosion scars, ephemeral gullies, and concentrated flow pathways with evidence of erosion; (2) we coupled the field disconnectivity assessment with GIS analyses to observe larger and more prominent landscape features that might also influence the connectivity, such as floodplains and karst sinkholes; (3) we used general knowledge of the system gathered from field visits and data collection the past three years of study from researchers at the University of Kentucky; and (4) we compared landscape features, land use, and erosion pathways visually using multiple sets of orthophotos from varying years, especially in regards to parameterizing the probability of non-hydrologic detachment component of the model.

After completing each site visit, we post-processed reach information on a geospatial database using a weighting and averaging technique to score qualitatively several watershed sedimentation parameters including erosion, deposition, and lateral and longitudinal disconnectivity. Conglomerate scores led to the development of hotspot maps. In particular, the presence of buffers such as floodplains, sinkholes, farm dams, and terraces within sub-reaches qualitatively determined lateral disconnectivity. We recognized the potential for subjectivity in the field assessment, and thus multiple researchers individually scored each parameter of the sub-reaches and the average of the researchers' scores was used to create the conglomerate hotspot maps for the major parameters assessed.

One main utility of the field assessment and geospatial analyses was to understand disconnectivity from floodplains and karst sinkholes. The land surface upstream of floodplain buffers was assumed disconnected from the stream network and thus not contributing to sediment flux at the watershed outlet. Approximately 5200 points simulated the extent of the delineated buffer features. Using ArcHydro, which is a set of data models that delineate and characterize watersheds in ArcMap (Maidment, 2002), and specifically the Batch watershed delineation tool, we determined the upstream contributing area of each point to delineate disconnected land. Another feature of potential sediment disconnectivity was water and sediment transport to karst sinkholes. Karst sinkholes are depressions leading to active or legacy (i.e., clogged) holes in the ground surface caused by cover collapse resulting from chemical dissolution of carbonate rock (Taylor, 1992). In the South Elkhorn, sinkhole drainage area can vary from a few square meters to as large as five hectares, where the former is from a relatively new cover collapse and the latter from successive dissolution and collapse leading to depression in the land surface. During rainfall events, runoff and eroded sediment can transport in the depressions and either deposit or enter the karst subsurface. We quantified the extent of the sinkhole drainage area in our study basin using published files from the USGS and the Kentucky Geological Survey (Currens et al., 2002; Taylor and Nelson, 2008; Zhu et al., 2014; KGS, 2017). Currens et al. (2002) as well as references cited therein performed extensive study of the karst features in the basin and surrounding watersheds over the course of a 25 year period. Sinkhole occurrence, drainage areas, and flow pathways

were mapped in a geospatial data file using dye trace studies, water-level data and inference, geologic structure, the existence of significant sinkhole and spring features, and delineation methods (Currens et al., 2002; Taylor and Nelson, 2008; Zhu et al., 2014). The karst geospatial data served to highlight the percent coverage of sinkholes and their pathways, and then we coupled the spatially explicit data with sediment connectivity modeling, as discussed later.

Additional hydrologic and geospatial data served as model inputs. A land cover map was coupled with soil survey data, as determined by the United States Department of Agriculture (USDA), and the Natural Resources Conservation Service (NRCS). A high-resolution DEM created by the Kentucky Aerial Photography and Elevation Data Program in 2014 (KYAPED, 2014) was used to predict the probability of connectivity at 1.5 m by 1.5 m. Practicality of using the high resolution DEM is a function of its availability and computational processing time. The high resolution DEMs are freely available for the entire state of Kentucky USA, where the study is performed. Simulation of the probability of connectivity model using a 1.5 m DEM for a 62 km<sup>2</sup> watershed for one year took 28 h on a desktop PC (Intel® Core™ i7-6700 CPU at 3.40 GHz; 64-bit operating system, x64-based processor). The computational time will increase with watershed scale, but the time could be offset with the use of parallel computing. A USGS gage located near the watershed provided discharge data from October 1, 2017, until the present. Turbidity and total suspended solids data were collected intermittently in the watershed since 2005. The National Oceanic and Atmospheric Administration (NOAA) maintains a precipitation and temperature monitoring station at the Lexington Bluegrass Airport located centrally in the watershed.

#### 3.3. Hydrologic modeling

We used an off-the-shelf hydrologic model deemed suitable for the study watershed to simulate the hydrologic connectivity. The Soil and Water Assessment Tool (SWAT) was developed (Arnold et al., 1998; Neitsch et al., 2011; SWAT 2012) to simulate the physical processes of water movement from different land uses and management practices at various watershed scales. We chose this model due to its past successful application in the central Kentucky USA region (Palanisamy and Workman, 2014; Al-Aamery and Fox, 2016) and its wide popularity.

Equation (3) represents the water balance equation used by SWAT to simulate the hydrologic cycle and is presented as:

$$SW_t = SW_0 + \sum_{i=1}^{t} (R_{day} - Q_{surface} - E_a - w_{seep} - Q_{gw})$$
(3)

where  $SW_t$  is the final soil water content on day t (mm of water);  $SW_0$  is the initial soil water content on day i (mm of water);  $R_{day}$  is the amount of precipitation on day i (mm of water);  $Q_{surface}$  is the amount of surface runoff on day i (mm of water);  $E_a$  is the amount of evapotranspiration on day i (mm of water);  $w_{seep}$  is the amount of lateral flow (interflow) on day i (mm of water); and  $Q_{\rm gw}$  is the amount of (return flow) on day i (mm of water). Hydrologic response units (HRUs) group landscapes with similar land uses, soil types, and slopes. SWAT outputs runoff, soil water content, and many other parameters for each HRU at the indicated time step. To simulate hydrologic connectivity, each of the 62 HRUs modeled within the Upper South Elkhorn were spatially mapped in ArcMap and model results were assigned as attributes. Output parameters from SWAT used in the probability of connectivity model include daily runoff and daily curve number for each HRU. Daily runoff for each HRU is determined using the NRCS Curve Number method (NRCS, 1972), which is shown in Eq. (4) as

$$Q_{surface} = \frac{(R_{day} - I_a)^2}{(R_{day} - I_a + S)} \tag{4}$$

where  $Q_{surface}$  is the accumulative surface runoff or rainfall excess on a day (mm of water),  $R_{day}$  is the depth of the rain on a day (mm of water),

S is the retention parameter (mm of water),  $I_a$  is the initial abstraction on a day (mm of water) and is generally estimated as 0.2S, the retention parameter (S) varies spatially due to changes in soil, land cover, and surface slope and temporally due to changes in soil water content. This parameter is explained as the following

$$S = 25.4 \left( \frac{1000}{CN} - 10 \right) \tag{5}$$

where CN is the curve number.

Semi-automatic calibration was adopted to calibrate the SWAT model for our watershed (Al-Aamery and Fox, 2016) on a daily basis. The focus of this paper investigates sediment mobility at the event time scale because sediment connectivity is a dynamic processes (Ambroise, 2004; Lexartza-Artza and Wainwright, 2009; Fryirs, 2013) and because of the event-based "pulses" of sediment transport that are important at the watershed scale (Fryirs, 2013). The Sequential Uncertainty Fitting SUFI2 of SWAT-CUP (Abbaspour et al., 2007a,b) was used to perform the calibration, sensitivity analysis and uncertainty of our results. The statistical metrics selected for this study to assess the simulated versus the observed streamflow were the coefficient of determination  $(R^2)$ , percent bias (PBIAS%), Nash-Sutcliff Efficiency (NSE) and the ratio of the root mean square error to the standard deviation of measured data (RSR) (Moriasi et al., 2007). The degree of uncertainty of the calibrated model was assessed using the P-factor and R-factor (SWAT, 2012). The parameters chosen for model evaluation were selected based on what was reported in previous studies (Arnold et al., 2012). Two years (2004-2005) of the SWAT simulation were treated as a warm-up period. The model evaluation was consistent with methods and results in Al-Aamery and Fox (2016). Model simulation from 2006 to 2010 served as the calibration phase while 2011 to 2013 served as the validation phase. Results from the model evaluation (see Table 3) showed the hydrologic model performed very well. Based on hydrologic model evaluation criteria outlined in Moriasi et al. (2007), the monthly time step model performance is considered satisfactory if the NS greater than 0.5, RSR less than 0.7, and PBIAS  $< \pm 25\%$ ; our simulation met all criteria in both calibration and validation. Model performance on daily time steps is expected to be poorer than the criteria set for monthly time steps, somewhat relaxing the mentioned thresholds (Moriasi et al., 2007, Engel et al., 2007). In the present case, the daily simulation meets the monthly threshold criteria further highlighting the very good performance of the model.

# 3.4. Probability of sediment connectivity modeling

We parameterized the individual probabilities in Eq. (2) as a set of discrete, piecewise distributions to represent small regions, or geospatial cells, of the watershed. The six probabilities were estimated for each geospatial cell, and the discretized results were later integrated to provide continuous distribution functions applicable to the entire watershed.

A simple piecewise function predicts the probability of sediment supply for a geospatial cell n as

$$P_i(S) = \begin{cases} 1, & \text{if sediment is present within the cell} \\ 0, & \text{if sediment is absent within the cell} \end{cases}$$
 (6)

**Table 3**Statistical metrics for calibration and validation of the hydrologic model.

Optimization Gage	Total Flow Calibration (For the period 1/1/2006–12/31/2010)			Total Flow Validation (For the period 1/1/2011–12/31/2013)				
	R <sup>2</sup>	RSR	PBIAS %	NS	R <sup>2</sup>	RSR	PBIAS %	NS
USGS- 03289000	0.61	0.66	18.43	0.56	0.76	0.56	5.5	0.69

where i is an index representing a geospatial cell. We parameterized equation (6) through observations, both from field visits and remote sensing, of the occurrence of a sediment surface that might be eroded. We consider erodible surfaces to be any pervious surface. Impervious surfaces were digitized using aerial imagery provided by the USDA National Agriculture Imagery Program (NAIP) in 2010. The digitization of the probability of sediment supply was converted into a raster with resolution of  $1.5\,\mathrm{m}$  by  $1.5\,\mathrm{m}$ .

We express the probability of hydrologic detachment using an excessive shear stress approach as

$$P_{ij}(D_H) = \begin{cases} 1, & \text{if } \tau_{fij} - \tau_{cri} > 0 \\ 0, & \text{if } \tau_{fij} - \tau_{cri} \le 0 \end{cases}$$
 (7)

where j is an index representing a time step. The probability of hydrologic detachment was a temporally varying probability because the runoff depth changes with time as function of the distribution of precipitation and soil conditions. Equation (7) evaluates the shear stress of the fluid in the geospatial cell,  $\tau_f$ , with respect to the critical shear stress. The shear stress of the fluid was approximated via the fluid momentum equation considering one-dimensional uniform flow (see Jain, 2001, pp. 58). The runoff depth of the geospatial cell for a given time step was estimated from the hydrologic model, the energy gradient was assumed the landscape slope determined in ArcMap. The critical shear stress of the sediment to resist erosion was parameterized by considering the soil characteristics and land management characteristics controlling the binding of particles into aggregates (Tisdall and Oades, 1982; Alberts et al., 1995; Foster et al., 1995; Lal, 1999). Critical shear stress was predicted using the empirical critical shear stress equation for rangeland soil (Alberts et al., 1995) as a function of texture, organic matter and soil bulk density, which were available in the soil geospatial layers from the USDA.

The probability of non-hydrologic detachment considers the presence of natural or anthropogenic disturbance agents, other than fluvial processes, that might initiate sediment detachment as

$$P_i(D_{NH}) = \begin{cases} 1, & \text{if a disturbance agent exists} \\ 0, & \text{if a disturbance agent is not present} \end{cases}$$
 (8)

Equation (8) is not dependent on watershed scale. However, thorough field or remote sensing observations of non-hydrologic disturbances that detach sediment from the soil surface must be identified to parameterize the probability of non-hydrologic detachment. Examples include livestock that trample and dislodge soil particles and mechanized detachment that might occur during construction. Farms with livestock nearby the stream corridor and construction sites were digitized in *ArcMap* and assumed to detach sediment.

Other non-hydrologic disturbances such as tillage, vehicle traffic, and mass wasting were not included in the analyses, which is a potential limitation of the study. However, we assumed tillage, vehicle traffic and mass wasting to be of small importance to sediment transport in this watershed for following reasons. Regarding tillage, almost all of the agriculture in the watershed is hay pasture, and cultivated crops account for less than 3% of the land cover (see Fig. 3). Of the existing cultivated crops, most of the row crops are grown with no-till, and the farming industry protects the cropland from erosion (Smallwood, 2017). Dirt roads and skidding trails have been shown to increase connectivity in forest regions (López-Vicente et al., 2017). In the present study, we do not expect roadways to cause sediment mobilization, other than water accumulation in ditches from roadway runoff. Based on our field assessment, there are no commonly used dirt roads in the watershed. Some gravel roads exist, but these are highly compacted. The agriculture lands had paved or gravel roads attributed to the profitable and optical equine industry. The agriculture of the basin is well-established pasture to serve the 3-billion-dollar equine industry in the Bluegrass, and the horse farms generally do a good job of maintaining their pastureland resource (ESR, 2013; Smallwood, 2017). The watershed falls within the low landslide incidence (less than 1.5% of the area involved) in the United States (Radbruch-Hall et al., 1982). We found no evidence of mass wasting in the basin during field assessments, which is consistent with the gently rolling topography.

We parameterize the probability for upstream hydrologic transport with the following piecewise function as

$$P_{ij}(T_{H-up}) = \begin{cases} 1, & \text{if } S_{aci} - S_{crij} > 0 \\ 0, & \text{if } S_{aci} - S_{crij} \le 0 \end{cases}$$
(9)

where  $S_{ac}$  indicates the slope of geospatial cell i and is assumed equal to the energy gradient and  $S_{cr}$  represents the critical slope required to initiate ephemeral gully incision of geospatial cell i (Montgomery and Dietrich 1994; Vandaele et al., 1996; Torri and Poesen, 2014). Equation (9) compares the actual slope ( $S_{ac}$ ) with the critical slope ( $S_{cr}$ ) to estimate the probability of upstream hydrologic transport. When  $S_{ac}$  of the land surface in the geospatial cell is greater than the  $S_{cr}$ , the probability is one for that individual cell. We parameterized  $S_{ac}$  using gradient analyses of a DEM. We parameterize  $S_{cr}$  using the equation of Vandaele (1993) as

$$S_{cri} = a_i A_i^{-b} \tag{10}$$

where a is a coefficient representative of the local climate and land use and soil characteristics of geospatial cell i, A is the upstream drainage area of geospatial cell i, and b is an exponent. The theory reflects the concept that the upstream drainage area may be a surrogate for the volume of concentrated surface runoff with sufficient magnitude and duration to sustain erosion (Vandaele, 1993). Torri and Poesen (2014) empirically derived a critical slope-upstream drainage area relationship for geospatial cells after extensively reviewing data collected by many researchers from 1983 to 2011 across six continents, and the relationship between critical slope and the upslope area was included here as

$$S_{crij} = 0.73c_i e^{1.3RFC_i} (0.00124S_{0.05ij} - 0.37) A_i^{-0.38}$$
(11)

where  $S_{0.05}$  represents the maximum potential loss to runoff as determined from the NRCS Curve Number (CN) method for a geospatial cell at a particular time step, RFC is the rock fragment cover of the soil, which affects the infiltration rate of runoff, and c represents other sources of the variation of the coefficient a from Equation (10) in geospatial cell i not accounted for by the CN approximation. Data from Torri and Poesen's (2014) study included numerous landscape features, ranging from rills to large ephemeral gullies. We included this equation in the model since these landscape features are known to facilitate sediment transport in the study basin. The CN method is assumed appropriate because runoff initiates in the silt loam soils, and the system as a whole is fluvial dominated. Sinkhole drainage areas cover 13% of the drainage basin, but the sinkhole flow pathways align well with the dendritic stream network. When runoff occurs, water is routed through sinkholes, to the shallow subsurface, and out springheads connecting to the stream. The CN method models the effect that vegetation, land use, and soil type have on runoff abstraction. Initial abstraction was predicted using the empirical equation developed by Hawkins et al. (2009)

$$S_{0.05} = 0.819 \left( 25.4 \left[ \frac{1000}{CN_{ij}} - 10 \right]^{1.15} \right)$$
 (12)

where  $CN_{ij}$  represents the Curve Number of cell i at time step j. The daily curve number output for individual HRUs via the SWAT hydrologic model represents  $CN_{ij}$ .

We parameterized the probability for downstream hydrologic transport as

$$P_{i}(T_{H-dwn}) = \begin{cases} 1, & if S_{i} - \frac{\sum S_{up}}{N} > 0\\ 0, & if S_{i} - \frac{\sum S_{up}}{N} \le 0 \end{cases}$$
 (13)

where  $S_i$ , representative of the slope in a particular geospatial cell, was found by applying the Slope tool in ArcMap to the Upper South Elkhorn DEM. *N* is representative of the number of upstream cells flowing into cell i, determined via the Flow Accumulation tool, which estimates the number of cells flowing into a downstream cell.  $\sum S_{uv}$  is the sum of the slopes of each cell upstream of cell i. This is determined by weighting the flow accumulation raster by the slope raster. In this manner, the fluid energy to transport sediment in cell *i* is compared to the incoming fluid energy. The probability of downstream hydrologic transport parameterization reflects the static connectivity of the watershed when surrogating slope for the energy gradient of the fluid. Note disconnected cells downstream of connected cells do not necessarily cause deposition. Rather, we imply that disconnected cells downstream of connected cells simply do not have the capacity to pick up more sediment that is contributable to the stream network. We believe this is reasonable considering very low gradient features causing deposition are explicitly included in the probability of buffers equation and the realization that fine sediments, once entrained, can take hours, or even days to settle (Jin and Romkens, 2001; Jin et al., 2002; Le Bissonnais et al., 2004; Owens et al., 2007; Liu et al., 2008; Rienzi et al., 2018).

The probability of non-hydrologic transport represents processes such as eolian transport and land sliding. However, the present application focuses on a fluvial-dominated system only; thus non-hydrologic transport was not parameterized.

We parameterize the probability of buffer disconnectivity as

$$P_i(B) = \begin{cases} 1, & \text{if a buffer exists} \\ 0, & \text{if abuffer does not exist} \end{cases}$$
 (14)

We identified features causing sediment disconnectivity via observations in the field assessment. If features did exist, the entire upstream region of the watershed that was disconnected was parameterized with P(B) = 1. However, we had uncertainty regarding the ability of karst sinkhole features to cause a net disconnectivity and act as buffers of lateral transport (i.e., P(B) = 1) within the basin. Sinkhole drainage areas are expected to pirate transported sediment or sediment may deposit in the surface depression itself similarly to the fallout of sediment transported from hillslopes to floodplains. Uncertainty of the disconnectivity occurs because pirated sediment may resurface at springheads and therefore the sediment may reconnect back to the fluvial network. Recent studies in the Inner Bluegrass have mixed results regarding springhead sediment production. For example, we analyzed karst spring sediment productivity from data reported in recent journal papers for the Inner Bluegrass (Reed et al., 2010; Husic et al. 2017a,b). Husic et al. (2017b) showed the Royal Spring to produce an order of magnitude lower sediment concentration than surface streams during hydrologic events of various magnitude. Reed et al. (2010) showed two springs in the region produced sediment concentrations on the same order of magnitude as surface streams, albeit they collected data from rather substantial hydrologic events with 4 to 6 cm of rainfall. In the South Elkhorn, the sinkhole drainage area is small (13% of the drainage area) relative to surrounding basins (see Table 2) but springhead sediment production may not be negligible. Therefore, we perform disconnectivity analyses and propagate the analyses through the probability of connectivity modeling by considering the sinkhole drainages as disconnected and separately analyzed the watershed considering the sinkholes as connected. The analyses provides upper and lower level uncertainty bounds on our results.

#### 3.5. Surface erosion modeling

The probability of sediment connectivity model provides the spatially explicit erosion features and the active contributing area for sediment transport in any time step. The erosion model simulates sediment yield at the watershed outlet by integrating the daily volume of eroded sediment from the active contributing area predicted by the

probability of connectivity model at the specified time step. Yearly sediment yield is predicted by integrating the daily sediment yield. Daily sediment yield was predicted as

$$S_{y} = \varepsilon \rho_{s} t l w \tag{15}$$

where  $S_y$  is the sediment yielded at the watershed outlet from the active contributing area (tonnes),  $\varepsilon$  is the erosion rate (m/s) as predicted by the Partheniades (1965) equation,  $\rho_s$  is the bulk density of the sediment (kg/m<sup>3</sup>), t is the amount of time sediment is contributed from the active contributing area (s), l is the length of the eroding rill or ephemeral gully (m), and w is the width of the eroding rill or ephemeral gully (m). We assume the erosion rate is proportional to shear stress in excess of the critical shear stress of the eroding surface, as predicted by Partheniades (1965), as

$$\varepsilon = k_d(\tau_f - \tau_{cr}) \tag{16}$$

where  $\varepsilon$  is the erosion rate of the soil (m/s),  $k_d$  is the erodibility coefficient (m³/N-s),  $\tau_{cr}$  is the critical shear stress of the eroding surface (Pa), and  $\tau_f$  is the effective shear stress (Pa) of the accumulated flow on the eroding surface. The effective shear stress of the accumulated flow on the eroding surface was approximated via the fluid momentum equation considering one-dimensional uniform flow of runoff and runoff depth was approximated using the Darcy-Weisbach approach (e.g., Jain, 2001). The inputs to the erosion model are shown in Table 4 and included the critical shear stress of the eroding surface, bathymetries, channel lengths, relative roughness of the channel, bulk density of the eroded sediment, storm length, the time sediment is produced from an eroding channel, and an erodibility coefficient.

We specified several parameters using literature-derived methods. Time of concentration was used as a surrogate for storm length when surface erosion was occurring. We applied three methods to estimate the storm length including the watershed lag method (Mockus, 1961), the velocity method (NRCS, 2010), and the Kirpich equation (Wanielista et al., 1997). Average rill and gully width were empirically parameterized using the equation developed by Nachtergaele et al., (2002). Erodibility,  $k_d$ , and critical shear stress,  $\tau_{cr}$ , of the eroding soil were parameterized *via* typical literature values (Alberts et al., 1995; Hanson and Simon, 2001). We applied the friction factor following the Colebrook-White equation. The relative roughness ranged between 10% and 20% of the flow depth.

To estimate the net erosion rate of the connected cells, cells were lumped into three discrete fractions based on upstream contributing area. A flow accumulation raster within the GIS model was multiplied

**Table 4** Erosion model inputs and parameters.

Parameter	Description	Value	Units
$A_1$	Contributing Area, Bin 1	116	m <sup>2</sup>
$A_3$	Contributing Area, Bin 2	951	$m^2$
$A_3$	Contributing Area, Bin 3	34,079	$m^2$
$ au_{cr}$	Critical Shear Stress	3.5	Pa
$S_1$	Longitudinal Slope, Bin 1	0.16	m/m
$S_2$	Longitudinal Slope, Bin 2	0.13	m/m
$S_3$	Longitudinal Slope, Bin 3	0.12	m/m
$w_1$	Channel Width, Bin 1	0.088	m
$w_2$	Channel Width, Bin 2	0.13	m
$w_3$	Channel Width, Bin 3	0.44	m
$\varepsilon/D$	Relative Roughness	0.1	Unitless
F	Darcy-Weisbach Friction Factor	0.102	Unitless
$\rho_d$	Bulk Density of Eroded Sediment	1400	kg/m <sup>3</sup>
$t_1$	Storm Length, Erosion Time Bin 1	0.0833	hr
$t_2$	Storm Length, Erosion Time Bin 2	0.25	hr
$t_3$	Storm Length, Erosion Time Bin 3	0.5	hr
$k_d$	Erodibility Coefficient	0.0055	cm <sup>3</sup> /N-s
$L_1$	Channel Length, Bin 1	Varies daily	m
$L_2$	Channel Length, Bin 2	Varies daily	m
$L_3$	Channel Length, Bin 3	Varies daily	m
$\rho_w$	Density of Fluid	1000	kg/m³

with the probability of sediment connectivity raster to estimate the upstream contributing area for each cell. We chose size fractions iteratively such that several orders of magnitude of upstream contributing area were represented. The average slope of the connected cells was estimated using the most connected day of the first study year. The accumulated flow rate was determined for each cell by multiplying the average upstream contributing area times the runoff depth at the particular time step, and then dividing by a representative storm length.

We performed data assimilation to reduce propagation of error from the water model to the sediment model. As mentioned, the hydrologic model performed very well (see Table 3). However, even when a hydrologic model performs very well, differences between point observation and point simulation of the model results will still occur. We did not want to propagate these differences through the sediment transport model, so we performed data assimilation for days when the predicted average flow rate differed by more than 30% of the actual average daily flow rate (Mahoney, 2017). In turn, the sediment model could better reflect the actual runoff of the individual day and reduce propagation of error to the sediment formulae.

We calibrated and validated the erosion model by comparing the prediction of daily sediment flux to sediment flux estimated via measurements at the watershed outlet. Sediment flux estimates were completed by Russo and Fox (2012) using automated sampling and the Einstein approach (Einstein, 1950). The model was iteratively calibrated so the predicted daily sediment flux matched as closely as possible with the observed sediment flux. Three hydrologic events were used to calibrate the model and two hydrologic events were used for validation (Mahoney, 2017). Calibration parameters that were adjusted included the erodibility coefficient,  $k_d$ , the critical shear stress of the eroding surface  $\tau_{cr}$ , the relative roughness of the channel surface  $\frac{\varepsilon}{D}$ , the length of storm, and the contribution time of sediment from the eroding surface. The coefficient of determination and the Nash-Sutcliff coefficient were optimized during calibration. Thereafter, annual sediment vield was compared with results from Russo (2009) for additional verification.

### 4. Results

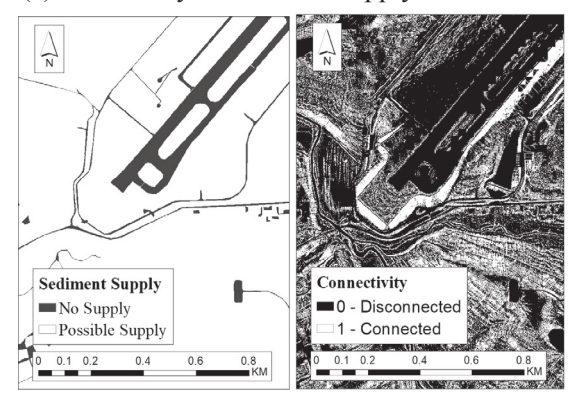
### 4.1. Evaluating model sensitivity

We investigated how each probability in Eq. (1) captured well-known erosion mechanisms to validate the probability of connectivity model was working well. Our validation was confirmed as shown in Fig. 4 where the individual probabilities predict disconnectivity from impervious surfaces with no sediment supply, low gradient surfaces with limited shear, surfaces towards the top of a slope length with limited flow accumulation, and surfaces upstream of buffers.

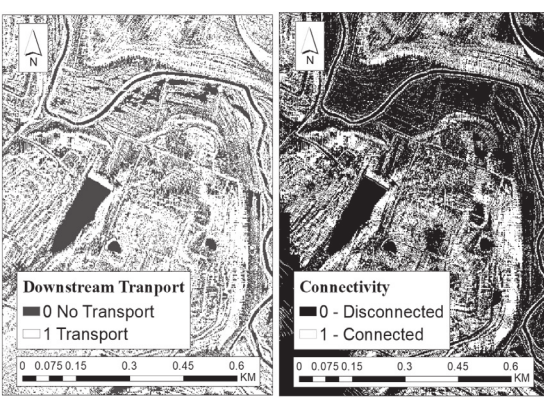
We next investigated the sensitivity of the individual probabilities to the results. Integration showed the probability of upstream transport exhibited the most control on the probability of connectivity, and this was true of both moderate and high rainfall events simulated throughout the model run (see Fig. 5). Differences in the results for moderate and high rainfall events show the dynamic nature of the probabilities of detachment and upstream transport, given their dependence on hydrologic connectivity. The probabilities of downstream transport, buffer disconnectivity, and supply are shown in Fig. 5 to be static given their dependence on the topography, morphologic features, and human-associated land cover. The dominant control of upstream transport in the present study qualitatively agrees with the high success of the Borselli et al. (2008) model founded on upstream transport. Nevertheless, the results in Fig. 5 show the importance of the other individual probabilities we included in our sediment connectivity model.

Our sensitivity analysis (Fig. 6) next focused on evaluating parameters in the model affecting the sediment connectivity including the

# (a) Probability of sediment supply

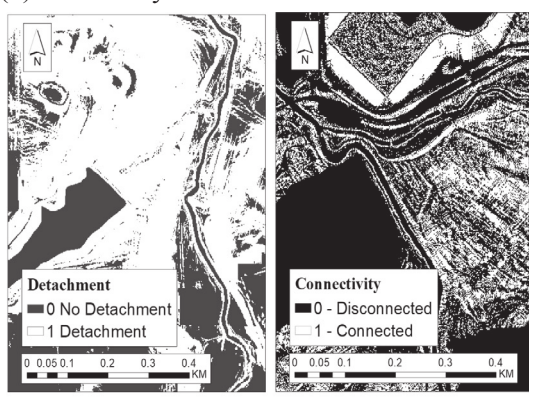


# (c) Probability of downstream transport



# (c) I robability of downstream transport

# (b) Probability of sediment detachment



# (d) Probability of upstream transport



# (e) Probability of buffers

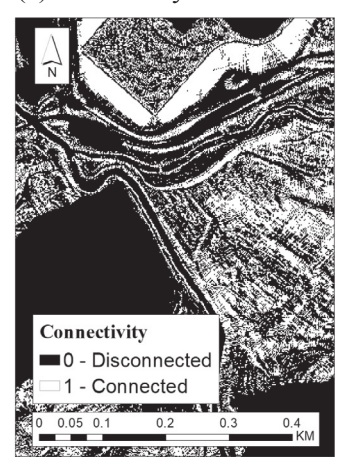


Fig. 4. Sediment erosion processes exemplified within probability of connectivity results.

critical shear stress and sediment transport coefficients, and results suggest our model parameterization is robust for the conditions of our application. The critical shear stress of sediment to resist detachment showed a lack of sensitivity until reaching a value of approximately 15 Pa (Fig. 6a), and critical shear stress parameterization beyond this threshold could reduce the sediment connectivity by as much as 100%. The high critical shear stresses reflect surface conditions more akin to vegetated channels and consolidated, stabilized bank soil conditions (Millar and Quick, 1998). The 15 Pa threshold is considerably higher than the critical shear stress expected for agricultural surface erosion processes (Alberts et al., 1995), and we do not expect such high critical shear stress conditions across the soils of the present study. The b exponent represents the flow condition to initiate erosion and showed a

lack of sensitivity until reaching very low values for the exponent of approximately 0.2. The very low threshold for sensitivity reflects conditions of viscous, laminar flow conditions. Results show that such laminar conditions would double sediment connectivity in the watershed, and these conditions reflect the dominance of pure sheet flow or perhaps pseudo-laminar flows with extremely high sediment concentrations. Nevertheless, we do not expect these conditions in the concentrated turbulent flow pathways to occur in the present study (Montgomery and Dietrich, 1994; Vandaele et al., 1996; Torri and Poesen, 2014). The *c* factor represents additional fluid and sediment pathways in the landscape that are not captured by the surface transport formula, and previous research emphasized the ability of the *c* factor to reflect piping. Torri and Poesen (2014) suggest a range of 0.1

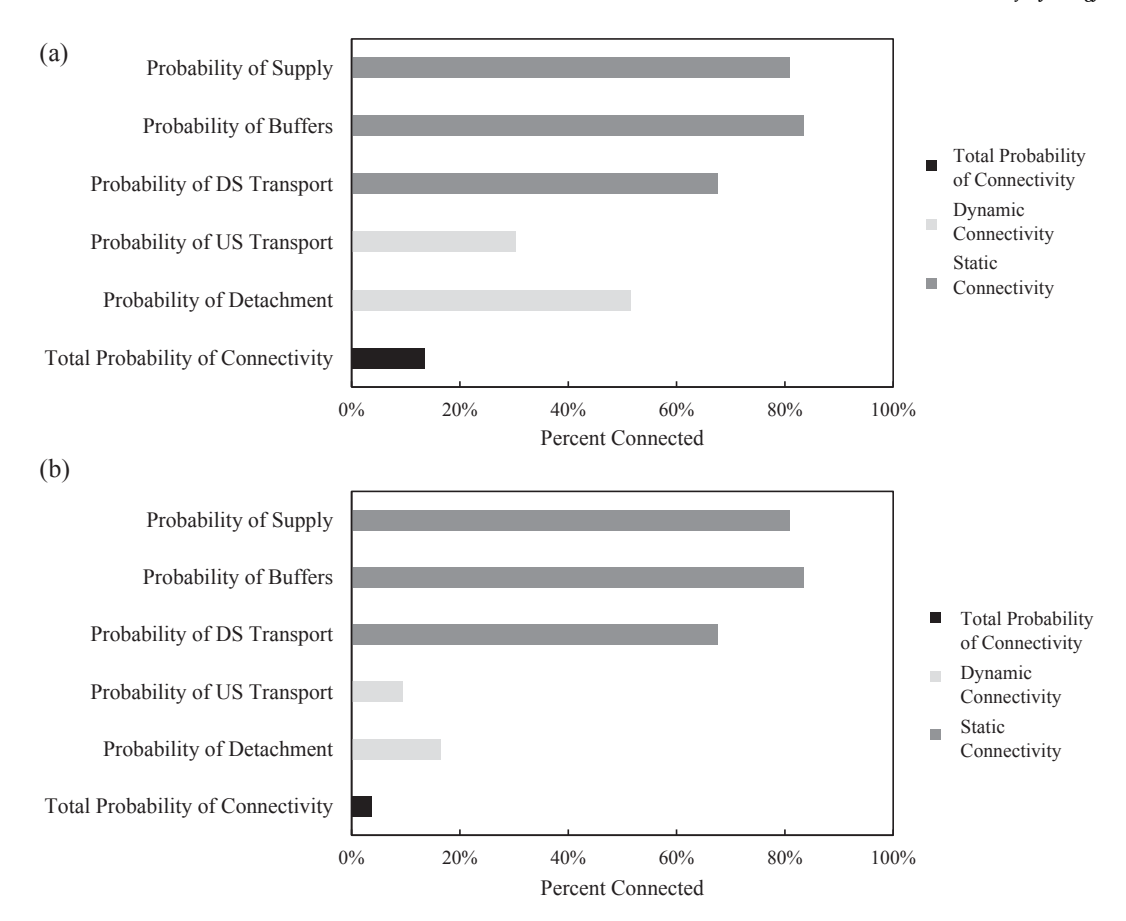


Fig. 5. Results of examples of net impact of individual probabilities upon the probability of sediment connectivity incorporating karst buffers. (a) Individual probabilities of connectivity for Day 128 within the simulation period.

to 0.4 reflects pronounced piping. Results show that a c factor in this range would nearly double sediment connectivity estimated from the model, although the South Elkhorn soils do not experience piping given the lack of soil texture variation vertically in the soil column (Fox et al., 2006). The South Elkhorn does have immature karst and 13% of the drainage area is sinkhole controlled. Rather than adjusting the c factor to try and account for the karst, we accounted for sinkholes within the probability of buffers term (see below for additional discussion of karst sinkholes).

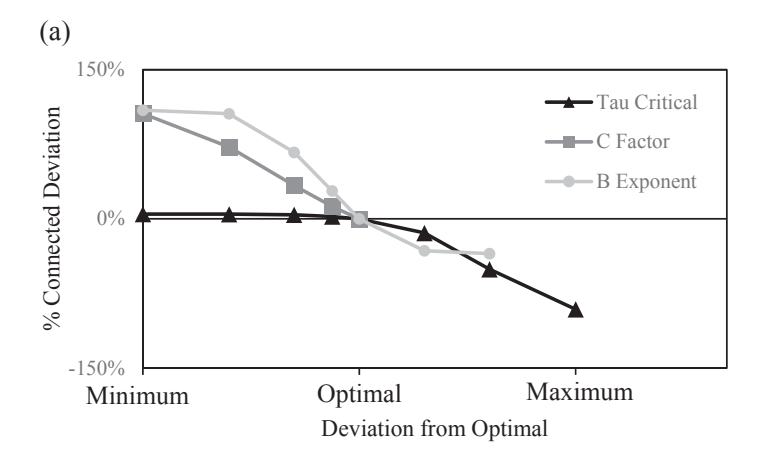
We next investigated the sensitivity of geospatial resolution upon the results. DEM resolution showed a substantial impact on the results. The 9 m by 9 m DEM estimated the probability of sediment connectivity to be nearly two times greater than the 1.5 m by 1.5 m DEM for the most highly connected days of the year (Fig. 6b). The sensitivity of the DEMs was a noteworthy result, and, on average, the deviation between the 1.5 m by 1.5 m and 9 m by 9 m DEM was 80%. The low-resolution DEM always estimated greater connectivity.

We carried forward the higher resolution, 1.5 m by 1.5 m, DEM when estimating sediment connectivity for several reasons. The higher resolution DEM better reflects the microtopography of the landscape and its ability, or lack thereof, to accumulate water, which agrees with recent sentiment by Cavalli et al. (2013) that higher resolution DEMs better reflect the actual landscape in connectivity studies. Visually, broad regions of connectivity and disconnectivity agree with one another for both the 1.5 m by 1.5 m and 9 m by 9 m DEMs (see Fig. 6c). However, results show the 1.5 m by 1.5 m DEM better captures the microtopography including steeper gradient swales where water accumulates before entering the stream while the 9 m by 9 m DEM masks across leads and ridges in the topography and treats entire sub-regions of the land surface as connected. Also, locally flat surfaces recognizable within the 1.5 m by 1.5 m DEM were masked in 9 m by 9 m DEM and

further increased the connectivity estimate. We inspected the results and found delineation of the landscape contributing area was one mathematical reason for higher connectivity estimates from the low-resolution DEM. As the upstream contributing area increases so too does the accumulated runoff to transport sediment in the ephemeral pathways of the uplands reflected *via* the probability of upstream transport. The lower resolution 9 m by 9 m DEM masks across locally flat surfaces in upstream geospatial scales and in turn increases the contributing area and the probability of connectivity.

We considered the sensitivity of karst sinkholes upon connectivity results. Sinkholes intercept approximately 13% of the watershed's drainage and are distributed throughout the landscape (see Fig. 7). We realized the potential importance of the sinkholes to impart sediment disconnectivity due to buffering lateral transport (i.e., P(B) = 1) because sinkhole drainage areas may pirate transported sediment or sediment may deposit within the surface depression. At the same time, pirated sediment may resurface at springheads and reconnect back to the fluvial network (i.e., P(B) = 0). This consideration was also deemed possible because dye traces showed that sinkhole pathways are consistent with the dendritic surface network in this watershed (see insert in Fig. 7). We considered a net disconnectivity versus net connectivity effect of the sinkhole drainage areas and found that the uncertainty from the karst features had a rather small effect on results. For example, the probability of connectivity varied from 12.1% to 13.5% on a wet day of the simulation period when including the karst uncertainty. The result is commensurate with the 13% coverage of sinkhole drainage in the South Elkhorn. At the same time, the results highlight the potential of karst sinkholes to cause sediment disconnectivity from microtopography. We include this uncertainty component by accounting for the range of results throughout the remainder of the paper.

Generally, predicted and observed daily sediment flux values



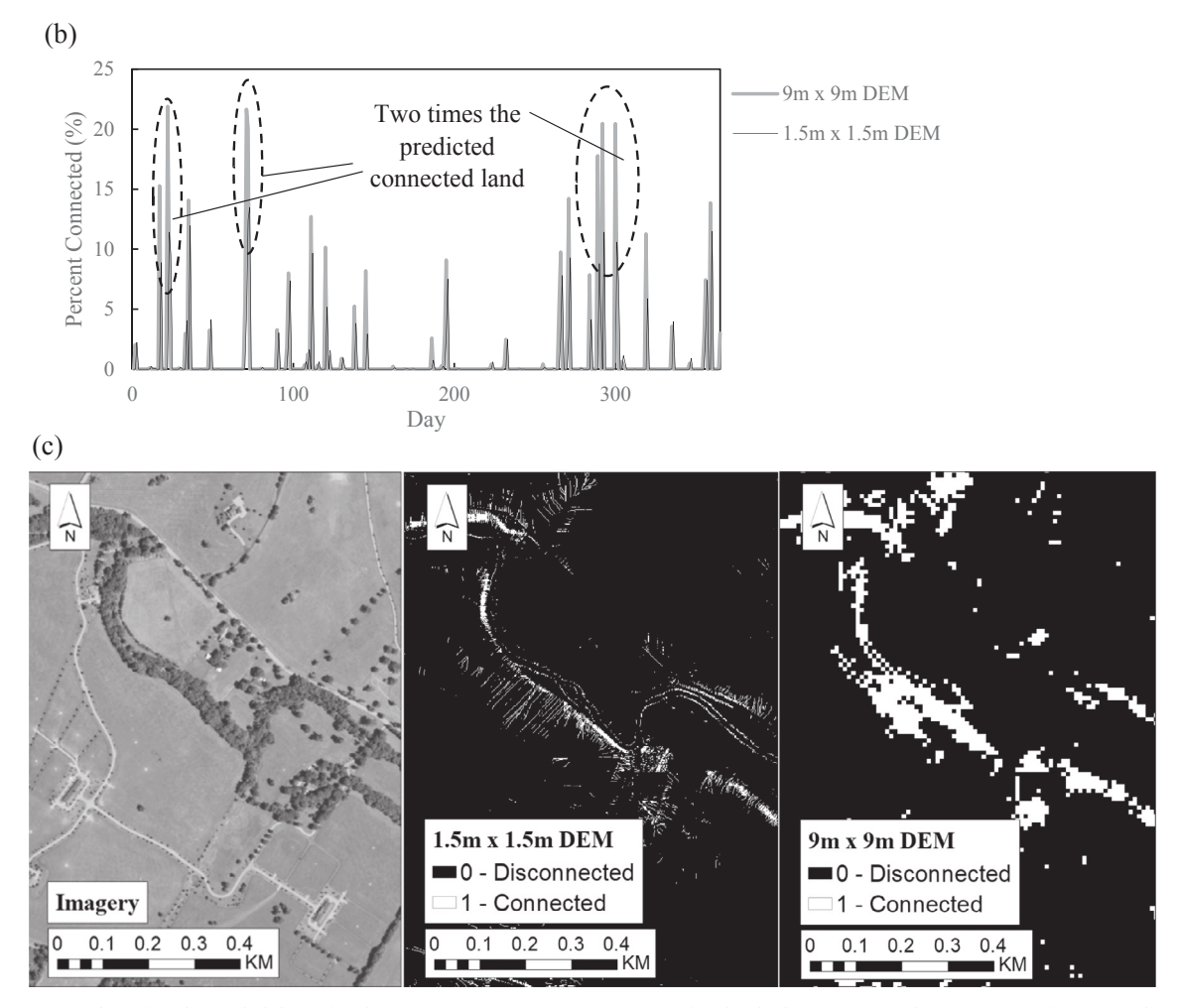


Fig. 6. Sensitivity analysis for the probability of sediment connectivity. (a) Sensitivity of individual parameters. (b) Sensitivity of geospatial resolution. (c) Comparison of the 1.5 m by 1.5 m DEM and the 9 m by 9 m DEM.

showed good agreement when comparing data and modeling results (Fig. 8a). Assimilation of hydrologic data during calibration and validation reduced the propagation of error from the hydrologic model to the watershed erosion model, and we found substantial differences in daily sediment flux when comparing assimilated and non-assimilated model runs (Fig. 8b). However, data assimilation did not affect net sediment yield results at the end of the simulation period. The results highlight the effectiveness of our data assimilation procedure for calibration purposes on an event-based daily to multi-day basis but also the

annual prediction capabilities of the watershed erosion model for times when data assimilation is not possible. Annual sediment yield for the watershed (3300  $\pm$  140 t y $^{-1}$ ) was 2% more than annual sediment yield estimated for the upland contribution reported in Russo and Fox (2012) for the same period, which provides further verification of the modeling results. Sensitivity analysis of parameters calibrated in the watershed erosion model showed the importance of the erodibility coefficient (Fig. 8c), which varies widely in the literature (e.g., review in Hanson and Simon, 2001). The time of concentration also showed

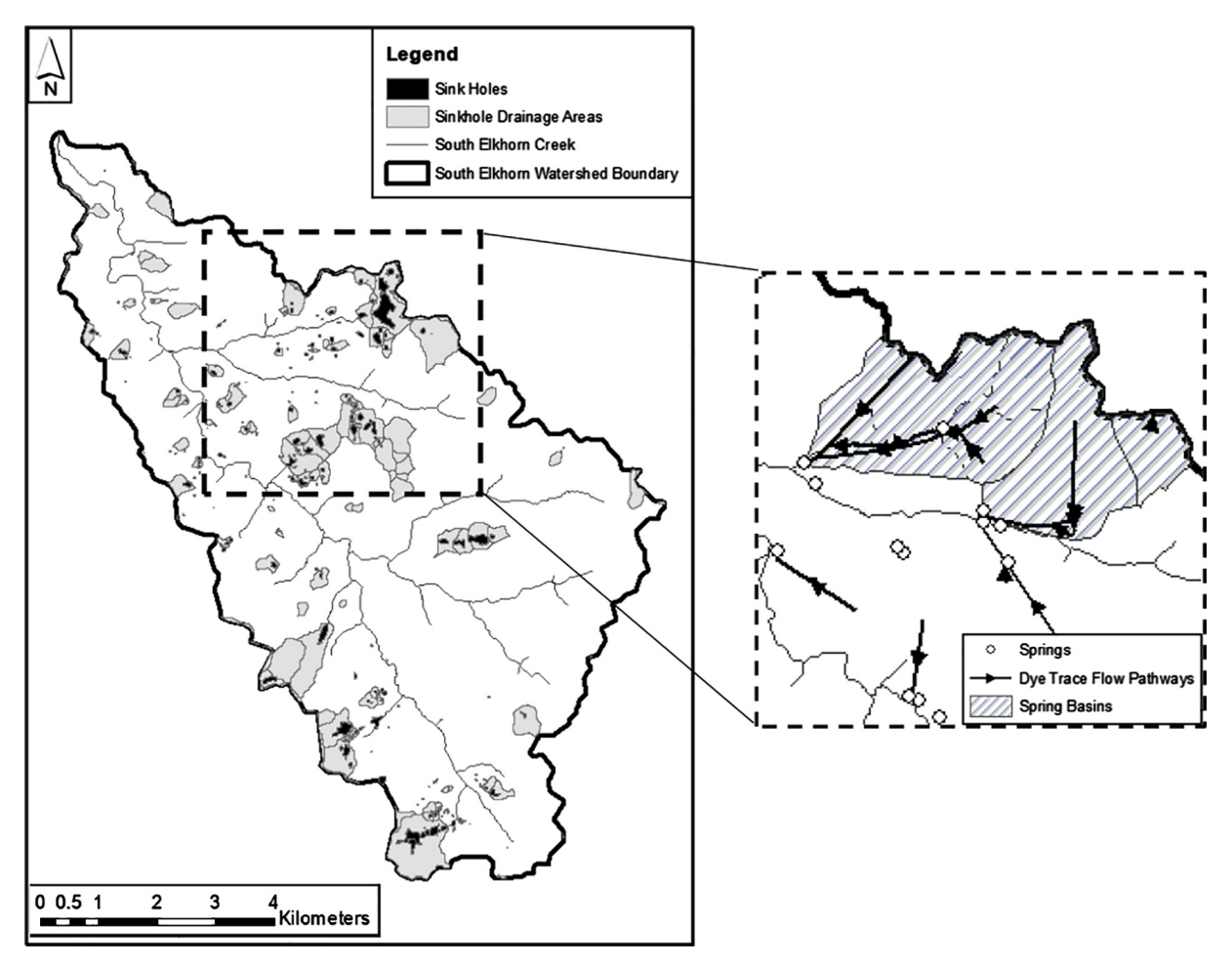


Fig. 7. Sinkhole map for the Upper South Elkhorn. Karst features drain 13% of the watershed area. The insert illustrates dye trace flow pathways performed by the Kentucky Geological Survey. Dye traces show that sinkhole pathways are consistent with the dendritic surface network, which emphasizes the fluvial dominance of this particular system. The South Elkhorn's immature karst is consistent with the findings of Phillips et al. (2004) for the Inner Bluegrass.

moderate sensitivity upon sediment flux while the impact of the friction coefficient and critical shear stress of sediment to resist erosion was marginal upon the sediment yield results.

#### 4.2. Watershed scale results

The probability of sediment connectivity varied throughout the year (Fig. 9) and reached a maximum value of 12.8  $\pm$  0.7%, on March 12 (day 72 of the study year) when high rainfall fell on wet soils. The results imply 12.8  $\pm$  0.7% of the watershed's surface had the potential to erode sediment on March 12. The mean sediment connectivity for the 104 days with some connectivity was 2.26  $\pm$  0.1% and the standard deviation was 3.5  $\pm$  0.15%. Sediment connectivity ranged from 0 to 1.5% for 67 of the 104 days and ranged from 1.7% to 13% for remaining 37 days (Fig. 10a). The beta distribution best fit the dynamic connectivity results. The beta distribution is a logical choice for representation of the dynamic probability given the beta distribution is continuous but bounded by 0 and 1, and therefore is suitable for representing the behavior of probabilities.

Results showed that the probability of sediment connectivity alone was not a good predictor of sediment flux. We highlight this idea in Fig. 10b, where temporal results are different for the probability of sediment connectivity and sediment flux. Obviously, sediment flux occurs only when some sediment connectivity exists; but sediment connectivity by itself does not predict sediment flux, as recently noted by Bracken et al. (2015).

Modeling results estimate that sediment connectivity was spatially

distributed across the watershed and that the northern region of the South Elkhorn Watershed exhibits the highest sediment connectivity. We attribute the spatially distributed results to a shift in the soil conditions in this region. Engineering properties of the soils shift from being dominated by moderately drained soils (i.e., NRCS hydrologic soil group B) in the southern and central regions of the watershed to dominated by poorly and very poorly drained soils (i.e., NRCS hydrologic groups C and D) in the northern region. The NRCS attributes the shift in the engineering properties to the decrease in percent sand and increase in percent fine clay in the northern region (NRCS, 2009). Sediment connectivity is slightly higher in the central-eastern region of the watershed relative to the central-western and southern regions. The result reflects the higher contribution of urban and suburban land uses in the central-eastern region, which in turn produce impervious surfaces, higher estimated runoff, and therefore higher values for the probability of hydrologic detachment and probability of upstream hydrologic transport.

We also assessed longitudinal variability of sediment connectivity by investigating the probability of sediment connectivity from catchment ( $\sim 1~\rm km^2$ ) to mid-sized watershed scales ( $\sim 60~\rm km^2$ ). Longitudinal variability results included a weak increase in the probability of sediment connectivity with scale (Fig. 10c), and the variance of sediment connectivity was highest at the smaller scale. The longitudinal variability of sediment connectivity reflects competing processes operating at different scales in a watershed configuration (Phillips, 2003; Borselli et al., 2008; Fryirs, 2013). Researchers suggest relatively steep land-scape gradients promote sediment connectivity at smaller scales such as

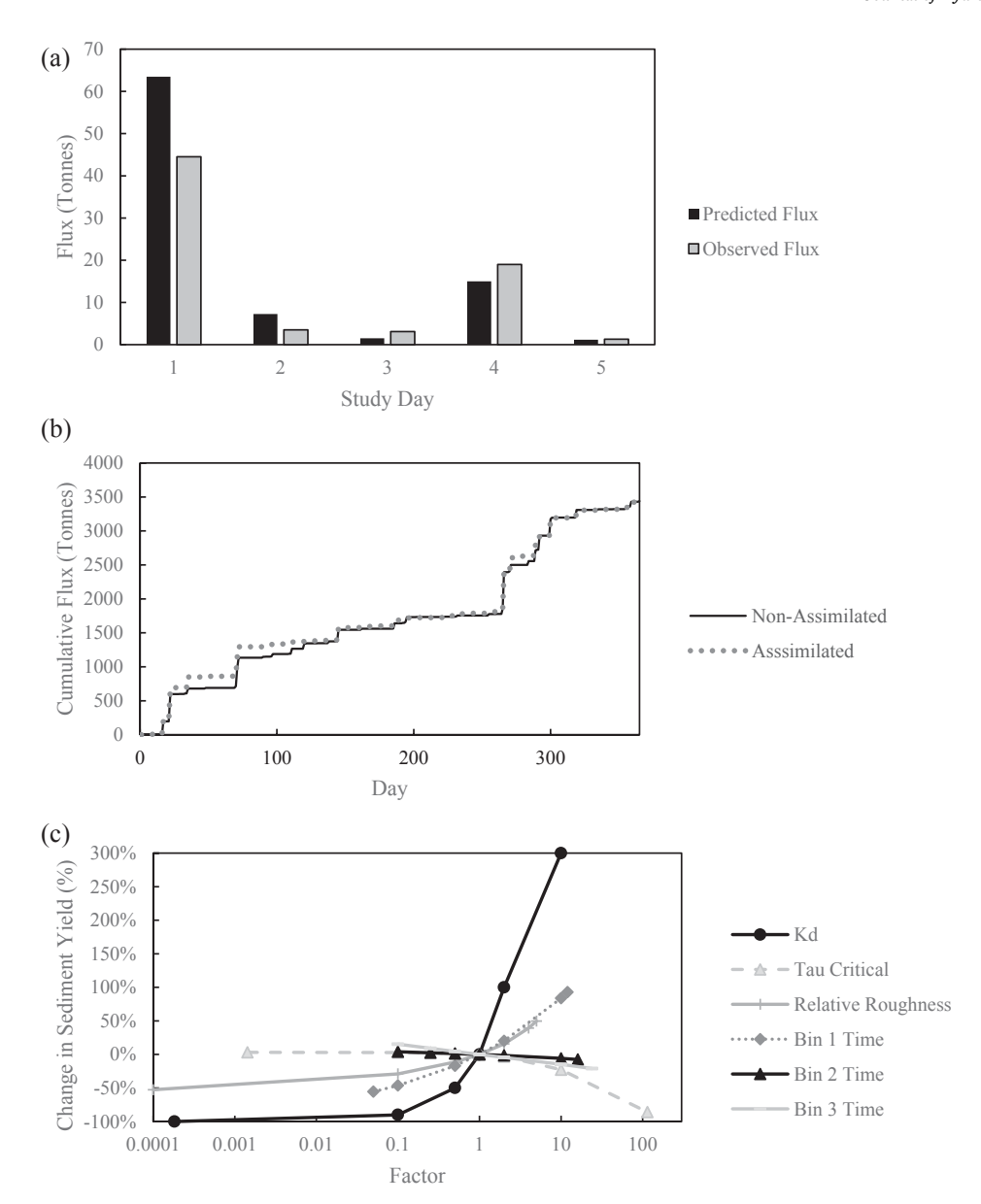


Fig. 8. Evaluation of the watershed erosion model results;  $R^2 = 0.95$ . (a) Predicted and observed sediment flux for specified days of the study period reflecting the upper limit where karst is assumed to be connected. (b) Sediment flux estimated with non-assimilated and assimilated streamflow data not accounting for the influence of karst. (c) Sensitivity analysis of parameters in the sediment transport model.

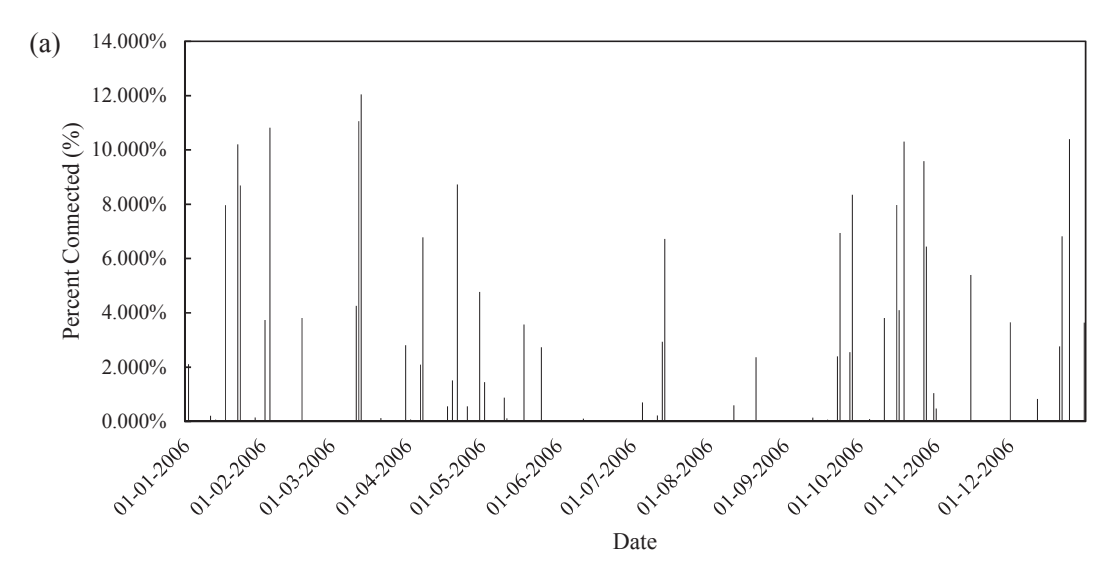
hillslope and small catchment scales (Fryirs et al., 2007). On the other hand, as the watershed scale increases, fluid accumulation has the potential to increase fluid shear stress and produce hydrologic connectivity for conveying sediment (Borselli et al., 2008). The weak power function result tends to suggest the latter process, i.e., flow accumulation, for the South Elkhorn, which we attribute to the dominance of erosion in concentrated flow pathways as opposed to sheet erosion processes.

## 4.3. Features of connectivity and disconnectivity

Unsurprisingly, sediment connectivity was high for the ephemeral network, steep slopes in newly constructed areas, ditches adjacent to roadways, and hillslopes adjacent to the stream (see Fig. 11). In turn, erosion-prone landscape features showed sediment flux from these sources, and the watershed erosion model results provided a spatially explicit estimate of erosion rates (see Fig. 12). The results further validated that our model was working well because past research has

suggested that erosion dominates from rill erosion, ephemeral gully erosion, and concentrated flow pathways in the watershed (Gumbert, 2017; Smallwood, 2017), and livestock and construction sites have been suggested to show increased detachment rates (Evans, 2017).

More surprisingly, sediment disconnectivity was dominated by microtopography across the gently rolling landscape. The greatest control on disconnectivity was the probability of upstream transport (Fig. 5), and upon further inspection of results from the high-resolution DEM, we found that the disconnectivity occurs because undulating land surfaces produces local low to zero gradient surfaces, i.e., flat slopes. The microtopography from the undulations causes small-sources of disconnectivity because runoff loses its energy in small depressions. Our field visits during storm events justified the geospatial model results. We found that even during intense rainfall events when runoff and flow accumulation were pronounced in ditches and swales, there was little to no runoff or sediment transport across pastureland surfaces and rather pooling within microtopographic depressions. The microtopography identified with the high-resolution DEM is noteworthy given the



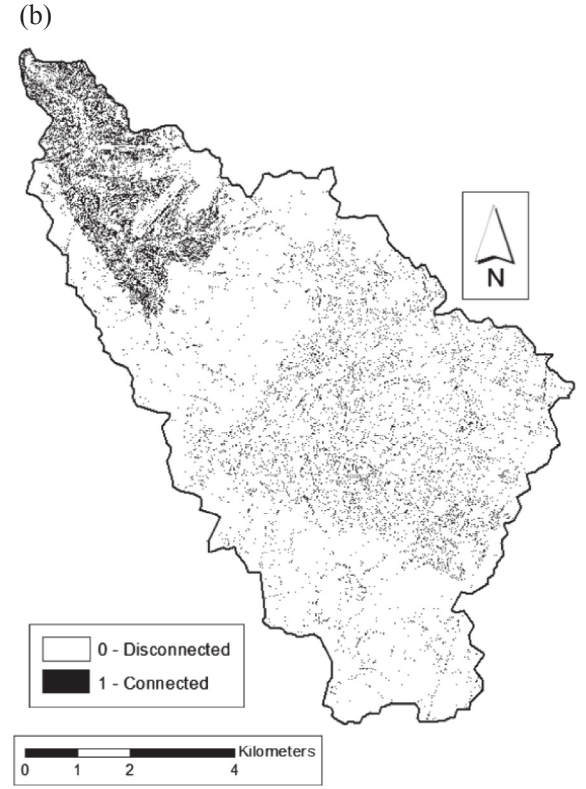


Fig. 9. Probability of sediment connectivity results for the South Elkhorn Watershed. (a) Probability of sediment connectivity results throughout one year reflecting the influence of karst. (b) Probability of sediment connectivity for March 12, 2006 (day 72).

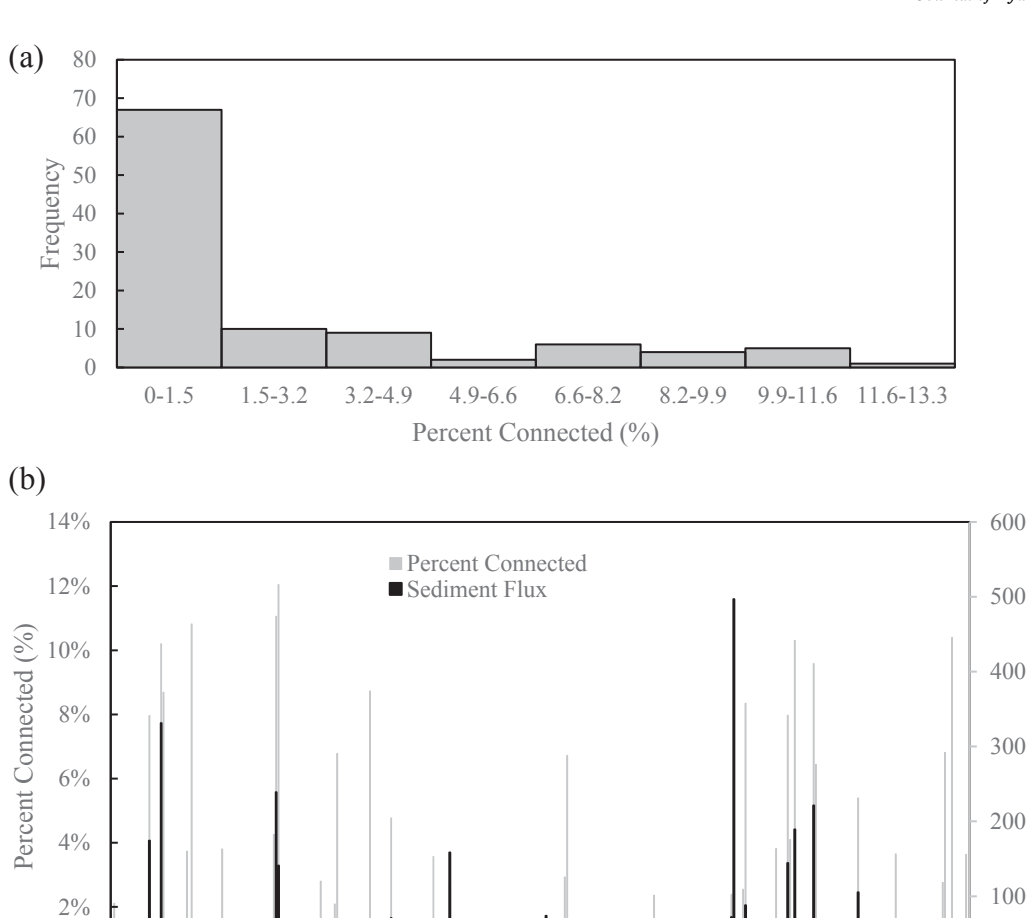
watershed itself was not flat (i.e., average hillslope gradient was 7%).

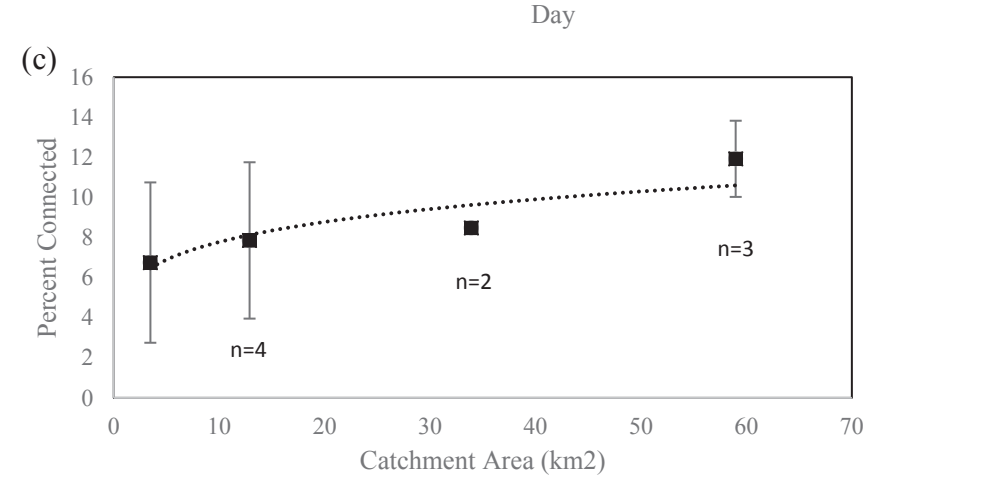
The potential of karst microtopography to impart disconnectivity is also noteworthy. Sinkhole microtopography may pirate transported sediment or cause fallout within depressions similarly to floodplain deposition, thus increasing lateral disconnectivity. While sinkhole impact was relatively small in this basin, sinkhole microtopography could potentially act as the dominant in neighboring basins in this region (see Table 2) as well as other regions with karst morphology.

Other recent studies corroborate the importance of microtopography upon sediment connectivity. Phillips et al., (2017) shows that microtopography associated with pits from tree uprooting and local surface armoring of rock fragments can disconnect erosion processes in an old-growth forest. Lopez et al. (2017) shows that a high-resolution DEM is useful to reveal how microtopography impacts

hydrological connectivity for roads and skidding trails in forest catchments. The usefulness of high-resolution DEMs is encouraging for sediment connectivity studies.

The floodplains are another disconnecting feature, yet the floodplains did not dominate disconnectivity as perhaps sometimes assumed. Based on our field assessment while walking the stream corridor, we initially presumed such a dominant behavior for the Upper South Elkhorn Watershed due to the prevalence of floodplains with flat gradients adjacent to the stream network. However, after completing the spatially explicit modeling, we found that floodplains buffered only 5% of the catchment. We recognized that the net effect of floodplains causes disconnectivity beyond the 5% measure due to the extension of low gradient surfaces forcing deposition of sediment from adjacent hillslopes draining to the floodplains. Nevertheless, the net effect of the





150

200

250

300

Fig. 10. (a) Frequency distribution for the probability of sediment connectivity (connected days only) accounting for influence of karst. (b) Results of percent connected versus sediment flux accounting for influence of karst. (c) Probability of sediment connectivity versus catchment area.

floodplains was only 35% disconnectivity, which was low relative to the probabilities of detachment, upstream transport, and downstream transport (i.e., 55 to 90% disconnectivity during hydrologic events, see example in Fig. 5b).

0%

0

50

100

# 5. Discussion

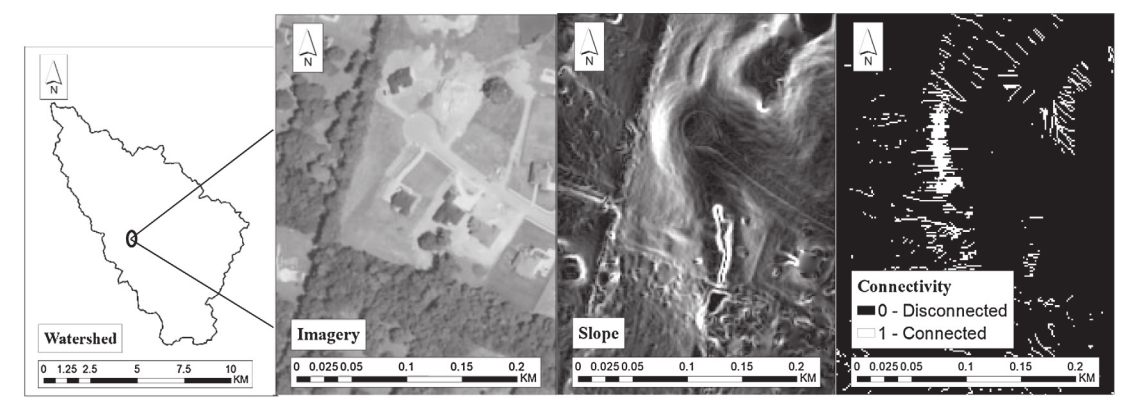
# 5.1. Spatially explicit and computational advancement of watershed erosion modeling

0

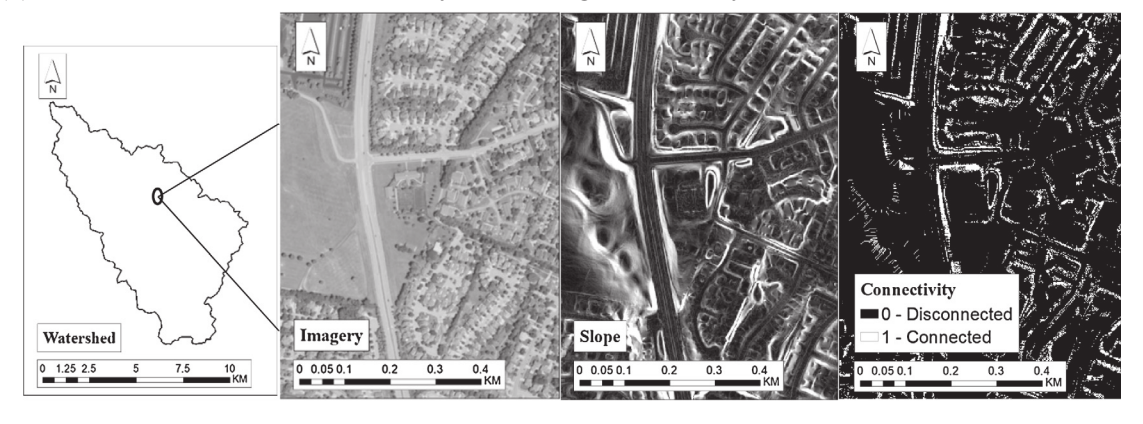
350

Our results show the efficacy of the probability of sediment connectivity approach to advance watershed erosion modeling for several reasons. First, results show that the approach accounts for spatial variability across the landscape by coupling the probability of sediment connectivity with the high-resolution digital elevation model (DEM).

# (a) Steep slopes in urban/newly constructed developments exhibiting connectivity



# (b) Water accumulation from roadways exhibiting connectivity



# (c) Agricultural concentrated flow pathways exhibiting connectivity

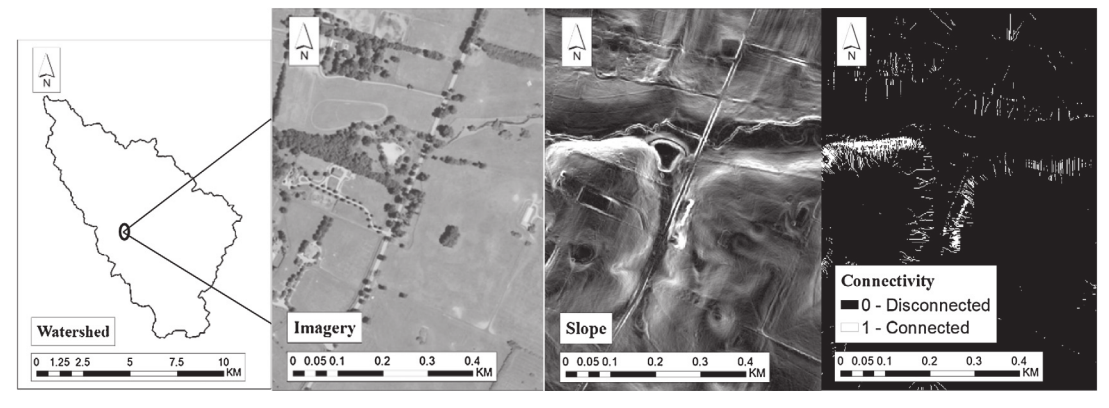


Fig. 11. Evaluation of the probability of sediment connectivity results by inspecting landscape features.

The high-resolution DEM helps resolve specific erosion features and sources, such as sediment connectivity around roadside ditches and disconnectivity from flat land surface gradients. In general, advantages of the 1.5 m by 1.5 m DEM suggest the researcher acquire the highest resolution DEM possible, which tends to agree with sentiment in the literature (Cavalli et al., 2013). However, some qualification is needed, and we suggest an upper limit is conceivable based on the underlying fluid mechanics assumptions. For example, calculations of both the probability of detachment and the probability of transport assume the landscape gradient equals the energy gradient of the fluid. These simplified representations assume the fluid mechanics in a geospatial cell

may be treated as uniform flow. The assumption is reasonable, albeit a recognized practical simplification, when the flow depth across the landscape is on the order of a few centimeters while the streamwise length scale is two orders of magnitude greater. The assumption may break down and require further investigation as to its sensitivity as the DEM resolution increases to a resolution of a few centimeters—a resolution that is no longer out of the question as technology continues to improve. In this case, the flow depth of runoff would be on the same order of magnitude as the resolution of the streamwise length scale, and individual large roughness elements act as hydraulic controls inducing non-uniformity to the flow. The landscape gradient in the profile of the

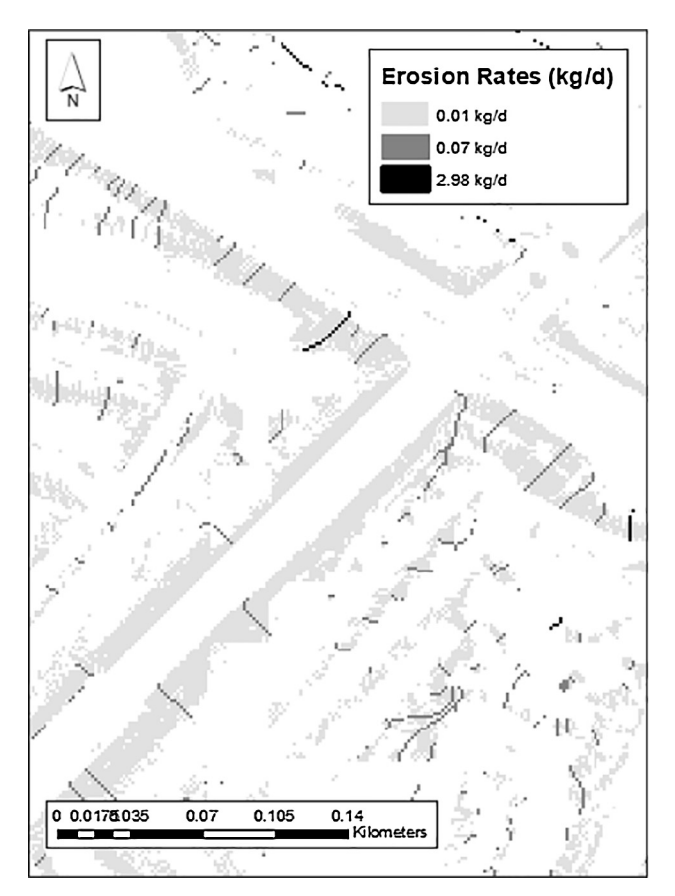


Fig. 12. Connected areas and the erosion rates for connected cells for a road network on day 72 of 2006.

hydraulic controls will be more extreme than the energy gradient of the flow. For example, an adverse landscape gradient has the potential to predict disconnectivity when the decelerating flow still has sufficient fluid shear stress to detach sediment. We point out that applying a very high, few centimeter resolution DEM in the probability of sediment connectivity does not negate the multiplicative theoretical basis for intersecting probabilities. However, researchers might consider parameterizing the flow as non-uniform across the landscape for such a high-resolution application.

Second, our results show that the watershed erosion model structure accounts for supply, shear, and transport criteria of sediment transport. Coupling sediment connectivity in watershed erosion models is a new area of research, and we suggest the approach provides the modeler with an added tool to account for sediment transport criteria via permutations of erosion formulae and connectivity principles. We highlight our model application as one such permutation. The model approach considers sediment supply limitations in a spatially explicit manner by calculating the probability of sediment supply using geospatial analyses. The approach considers transport limitations explicitly by calculating upstream and downstream probabilities of transport at each cell (see Fig. 4) and by identifying buffer discontinuities using field reconnaissance. With supply and transport accounted, we emphasized the shear limitation when coupling to the surface erosion formulae. We maximized the advantages of the spatially explicit datasets and the quantitative hydraulic formulae when considering shear, supply and transport limitations for the specific conditions of our system. We expect researchers may find many other permutations of erosion formulae and connectivity principles in future modeling of watershed erosion.

Third, we highlight that reducing the cost of computational hydrology is another attractive feature of a connectivity-based watershed erosion model. In the present application, the watershed modeling

included calculations for  $3 \times 10^{10}$  space-time combinations. The probability of sediment connectivity subroutine added explicit formulae to the watershed erosion model, and a geospatial modeling software performed calculations requiring several hours to run on a desktop PC. Considering all space-time combinations in the watershed modeling, only 0.7% of the combinations contained connectivity. Therefore, the model carried forward only  $2 \times 10^8$  space-time combinations in the hydraulic and sediment transport formulae and removed  $2.98 \times 10^{10}$ space-time calculations. Hydraulic calculations are often computationally intensive requiring solution of implicit formulae at each space-time step. Computational sediment transport is even more demanding as higher dimensional formulae (e.g., see above discussion of flow nonuniformities) and as researchers implement advanced routing methods. Thus, we suggest the inclusion of the connectivity-based watershed erosion model may have a net reduction in overall computational complexity. Further, the connectivity-based watershed erosion model provides the flexibility to include advanced computational complexity. Simulation of the breach of a buffer within the watershed configuration (e.g., see descriptions in Bracken et al., 2015) allows calling up sophisticated hydraulic and sediment subroutines that could simulate such spatiotemporal feedback and connectivity between sediment sources and sinks.

#### 5.2. Extending our view of sediment disconnectivity and connectivity

The newly quantified features of the gently rolling watershed complement existing knowledge and extend our view of disconnectivity. Our results agree with the concept that the gently rolling watershed morphology includes relatively stable land surfaces, ephemeral flow pathways, and the presence of decoupled floodplains (Jarrit and Lawrence, 2007; Ford and Fox, 2014) that can lead to trapping of as much as 90% of mobilized sediments in disconnected land surfaces (Meade et al., 1990; Hupp, 2000; Walling et al., 2006). Our results reflect this idea and show spatial disconnectivity on the order of 90% on the wettest day of the year. Microtopography across the landscape dominates disconnectivity because local low to zero gradient surfaces cause the ponding of runoff and sediment deposition in the undulating landscape. Our result is corroborated by past studies where sediment erosion from diffusive processes on land surfaces of the uplands only travel a spatial scale of several meters or less (Roering et al., 1999) as well as by recent results highlighting the influence of microtopography in forest catchments (Lopez et al., 2017; Phillips et al., 2017). Karst microtopography and the ability of sinkholes to pirate transported sediment and cause lateral disconnectivity is also noteworthy for the gently rolling watershed. The ephemeral network represents the most connected morphology of the uplands; however, disconnectivity persists through much of the ephemeral network even during high magnitude events. Floodplains cause lateral disconnectivity due to their potential to break connectivity between the ephemeral network and main channel, which is consistent with the work of others (Goudie, 2004; Florsheim et al., 2006; Kronvang et al., 2007; Jaeger et al., 2017).

Only about 10% of the uplands showed lateral sediment connectivity with the stream for the gently rolling watershed, which contrasts steeper gradient systems where connectivity results are much higher, e.g., Fryirs et al. (2007). Fryirs et al. (2007) predicted the active contributing area for four landscape units in the upper Hunter catchment in Australia, which have relatively high elevation, deep dissection, and a rugged, hilly landscape. Nearly 50% of the catchment was connected for a moderate storm event, which contrasts greatly with our gently rolling results of 10% connectivity for one of the most hydrologically intensive days of the year. We caution fine scale quantitative comparisons of papers given the modeling approaches applied and DEM resolution applied. Nevertheless, we mention the vast differences in connectivity that cast gently rolling watersheds as event-resilient, disconnected systems.

Regarding sediment connectivity, one potentially interesting result is the net importance of ditches and roadside gullies in the urban regions. The urban regions showed net higher connectivity than surrounding agricultural regions. The importance of roadways to induce erosion and sediment connectivity has been discussed previously for mountainous catchments (Latocha, 2014), and urban sprawl, i.e., urbanization, has been well understood to induce gully formation and channeling processes (Trimble, 1993). However, few papers to our knowledge have reported the net importance of roadway ditches and gullies in well-established urban environments. More generally, these ephemeral networks of urban and suburban regions may exhibit more sediment connectivity than agricultural regions in gently rolling systems, given the presence of a higher concentration of impervious surfaces and the well-defined drainage network promoting flow accumulation. The exception would likely be poorly managed watersheds where agricultural best management practices have yet to be adopted.

#### 6. Conclusions

Model evaluation results verify the capability of the probability of sediment connectivity to be integrated within watershed erosion modeling. The modeling approach accounts for the spatial variability of sediment connectivity across the landscape, and high-resolution DEMs were able to predict erosion features impacting sediment connectivity and disconnectivity. We suggest this approach provides the modeler with an added tool to account for sediment transport criteria given that each of the individual sediment probabilities exhibit some importance and coupling with erosion formulae provides sediment flux estimates. We also highlight the potential ability of the approach to reduce the cost of computational hydrology as modeling tools rely more-and-more on high-resolution prediction.

In the gently rolling watershed, results show that sediment connectivity occurs within ephemeral pathways across the uplands, but disconnectivity dominates the watershed configuration both spatially and temporally. All morphologic levels of the uplands exhibit disconnecting features including microtopography causing low energy undulating surfaces, karst sinkholes disconnecting drainage areas, and floodplains that de-couple the hillslopes from the stream corridor. Only  $12.8 \pm 0.7\%$  of the gently rolling watershed shows sediment connectivity on the wettest day of the year. Spatially, results highlight the importance of sediment connectivity in urban and suburban pathways given the well-defined channel network and influence of impervious surfaces. Dynamic and longitudinal results suggest the beta distribution and power function, respectively, might be further investigated for their ability to reflect the gently rolling watershed's connectivity more generally.

# Acknowledgements

We thank an anonymous reviewer for comments that helped us to improve greatly the quality of the work. We gratefully acknowledge the financial support of this research under National Science Foundation Award 163288.

#### References

- Abbaspour, K.C., Vejdani, M., Haghighat, S., (2007, December). SWAT-CUP calibration and uncertainty programs for SWAT. In: MODSIM 2007 International Congress on Modelling and Simulation, Modelling and Simulation Society of Australia and New Zealand, pp. 1596–1602.
- Abbaspour, K.C., Yang, J., Maximov, I., Siber, R., Bogner, K., Mieleitner, J., Srinivasan, R., 2007a. Modelling hydrology and water quality in the pre-alpine/alpine Thur watershed using SWAT. J. Hydrol. 333 (2), 413–430.
- Al-Aamery, N., Pox, J.F., 2016. Evaluation of Climate Modeling Factors Impacting the Variance of Streamflow. J. Hydrol. 542, 125–142.
- Alberts, E.E., Nearing, M.A., Weltz, M.A., Risse, L.M., Pierson, F.B., Zhang, X.C., Laflen, J. M., Simanton, J.R., 1995. Chapter 7 Soil Component. In: Flanagan, D.C., Nearing, M. A. (Eds.) USDA. Water erosion and prediction project hillslope profile and watershed

- model documentation, NSERL Report No. 10 USDA-ARS National Soil Erosion Research Laboratory, West Lafayette, Indiana 47907.
- Ambroise, B., 2004. Variable 'active' versus 'contributing' areas or periods: a necessary distinction. Hydrol. Process. 18 (6), 1149–1155.
- Arnold, J.G., Srinivasan, R., Muttiah, R.S., Williams, J.R., 1998. Large area hydrologic modeling and assessment part I: model development. JAWRA J. Am. Water Resour. Assoc. 34 (1), 73–89.
- Arnold, J.G., Moriasi, D.N., Gassman, P.W., Abbaspour, K.C., White, M.J., Srinivasan, R., Kannan, N., 2012. SWAT: Model use, calibration, and validation. Trans. ASABE 55 (4) 1491–1508
- Baban, S.M., Yusof, K.W., 2001. Modelling soil erosion in tropical environments using remote sensing and geographical information systems. Hydrological sciences journal 46 (2), 191–198.
- Borselli, L., Cassi, P., Torri, D., 2008. Prolegomena to sediment and flow connectivity in the landscape: a GIS and field numerical assessment. Catena 75 (3), 268–277.
- Bracken, L.J., Croke, J., 2007. The concept of hydrological connectivity and its contribution to understanding runoff-dominated geomorphic systems. Hydrol. Process. 21 (13), 1749–1763.
- Bracken, L.J., Turnbull, L., Wainwright, J., Bogaart, P., 2015. Sediment connectivity: a framework for understanding sediment transfer at multiple scales. Earth Surf. Proc. Land. 40 (2), 177–188.
- Brierley, G., Fryirs, K., Jain, V., 2006. Landscape connectivity: the geographic basis of geomorphic applications. Area 38 (2), 165–174.
- Brunsden, D., 1993. Barriers to geomorphological change. Landscape sensitivity, p. 675.
   Burns, R.G., 1979. An improved sediment delivery model for Piedmont forests. Georgia Inst. Technol, Atlanta, Ga.
- Cavalli, M., Trevisani, S., Comiti, F., Marchi, L., 2013. Geomorphometric assessment of spatial sediment connectivity in small Alpine catchments. Geomorphology 188, 31–41.
- Celik, I., Rodi, W., 1988. Modeling suspended sediment transport in nonequilibrium situations. Journal of Hydraulic Engineering 114 (10), 1157–1191.
- Cheng, N.S., Chiew, Y.M., 1998. Pickup probability for sediment entrainment. Journal of Hydraulic Engineering 124 (2), 232–235.
- Chorley, R.J., Kennedy, B.A., 1971. Physical geography: a systems approach. Prentice
- Croke, J., Fryirs, K., Thompson, C., 2013. Channel-floodplain connectivity during an extreme flood event: implications for sediment erosion, deposition, and delivery. Earth Surf. Proc. Land. 38 (12), 1444–1456.
- Currens, J.C., Paylor, R.L., Ray, J.A., 2002. Mapped karst groundwater basins in the Lexington 30 x 60 minute quadrangle. Kentucky Geological Survey, University of Kentucky, Lexington, KY USA.
- Davis, C.M., 2008. Sediment fingerprinting using organic matter tracers to study streambank erosion and streambed sediment storage processes in the South Elkhorn Watershed. M.S. Dissertation, University of Kentucky, Lexington, Kentucky.
- De Vente, J., Poesen, J., Verstraeten, G., 2005. The application of semi-quantitative methods and reservoir sedimentation rates for the prediction of basin sediment yield in Spain. J. Hydrol. 305 (1), 63–86.
- Dietrich, W. E., Dunne, T., Humphrey, N. F., & Reid, L. M. (1982). Construction of sediment budgets for drainage basins. Sediment Budgets in Forested Drainage Basins. United States Forest Service Gen. Tech. Rep. PNW-141. p5-23.
- Einstein, H.A., 1950. The bed-load function for sediment transportation in open channel flows Vol. 1026 US Department of Agriculture, Washington DC.
- Engel, B., Storm, D., White, M., Arnold, J., Arabi, M., 2007. A hydrologic/water quality model applicati1. Journal of the American Water Resources Association 43 (5), 1223–1236
- ESR-Equine Survey Report (Released September 6 2013), 2013. 2012 Kentucky Equine Survey. University of Kentucky Agriculture Equine Program, Lexington, Kentucky. Evans. S. Personal Communication. March 20. 2017.
- Ferguson, R.I., 1981. Channel form and channel changes. British Rivers 90, 125. Florsheim, J.L., Mount, J.F., Constantine, C.R., 2006. A geomorphic monitoring and adaptive assessment framework to assess the effect of lowland floodplain river response.
- adaptive assessment framework to assess the effect of lowland floodplain river restoration on channel–floodplain sediment continuity. River Res. Appl. 22 (3), 353–375.
- Ford, W.I., Fox, J.F., 2014. Model of particulate organic carbon transport in an agriculturally impacted stream. Hydrol. Process. 28 (3), 662–675.
- Ford, William Isaac III., 2011. Particulate organic carbon fate and transport in a lowland, temperate watershed. University of Kentucky Master's Theses. p. 647. http://uknowledge.uky.edu/gradschool\_theses/647
- Ford, William I. III., 2014. Control of the surficial fine-grained laminae upon stream carbon and nitrogen cycles. Theses and Dissertations–Civil Engineering. p. 21. http://uknowledge.uky.edu/ce\_etds/21
- Foster, M., & Fell, R. (2000). Use of event trees to estimate the probability of failure of embankment dams by internal erosion and piping. In Transactions of the International Congress on Large Dams (Vol. 1, pp. 237-260).
- Foster, M., & Fell, R. (2000). Use of event trees to estimate the probability of failure of embankment dams by internal erosion and piping. In Transactions of the International Congress on Large Dams (Vol. 1, pp. 237-260).
- Foster, G.R., Flanagan, D.C., Nearing, M.A., Lane, L.J., Risse, L.M., Finkner, S.C., 1995, Chapter 11. Hillslope erosion component, In: Flanagan, D.C., Nearing, M.A. (Eds). USDA – Water erosion and prediction project hillslope profile and watershed model documentation, NSERL Report No. 10 USDA-ARS National Soil Erosion Research Laboratory, West Lafayette, Indiana 47907.
- Fox, J.F., Davis, C.M., Martin, D.K., 2010. Sediment source assessment in a lowland watershed using nitrogen stable isotopes. JAWRA J. Am. Water Resour. Assoc. 46 (6), 1192-1204
- Fox, G.A., Sabbagh, G.J., Chen, W., Russell, M.H., 2006. Uncalibrated modelling of

- conservative tracer and pesticide leaching to groundwater: comparison of potential Tier II exposure assessment models. Pest Manage. Sci. 62 (6), 537-550.
- Fry, J., Xian, G., Jin, S., Dewitz, J., Homer, C., Yang, L., Barnes, C., Herold, N., Wickham, J., 2011. Completion of the 2006 National Land Cover Database for the Conterminous United States. PE&RS 77 (9), 858-864.
- Fryirs, K., 2013. (Dis) Connectivity in catchment sediment cascades: a fresh look at the sediment delivery problem. Earth Surf. Proc. Land. 38 (1), 30-46.
- Fryirs, K.A., Brierley, G.J., Preston, N.J., Spencer, J., 2007. Catchment-scale (dis) connectivity in sediment flux in the upper Hunter catchment, New South Wales, Australia. Geomorphology 84 (3), 297-316.
- Gessler, J., 1970. Self-stabilizing tendencies of alluvial channels. Journal of the Waterways, Harbors and Coastal Engineering Division 96 (2), 235-249.
- Glymph, L.M., 1954. Studies of sediment yields from watersheds. Int. Assoc. Hydrol. Sci. Publ. 36, 261-268.
- Goudie, A. (Ed.), (2004). Encyclopedia of geomorphology (Vol. 2). Psychology Press. Govindaraju, R.S., 1998. Effective erosion parameters for slopes with spatially varying properties. Journal of irrigation and drainage engineering 124 (2), 81-88.
- Govindaraju, R.S., Kavvas, M.L., 1992. Characterization of the rill geometry over straight hillslopes through spatial scales. Journal of Hydrology 130 (1-4), 339-365.
- Grass, A.J., 1970. Initial instability of fine bed sand. Journal of the Hydraulics Division 96
- Gumbert, A., 2017. Personal Communication. February 21, 2017.
- Hanson, G.J., Simon, A., 2001. Erodibility of cohesive streambeds in the loess area of the midwestern USA. Hydrol. Process. 15 (1), 23-38.
- Harvey, A.M., 1996. Holocene hillslope gully systems in the Howgill Fells, Cumbria. Adv. Hillslope Process. 2, 731-752.
- Haschenburger, J.K., 1999. A Probability model of scour and fill depths in gravel-bed channels. Water Resources Research 35 (9), 2857-2869.
- Hawkins, R.H., Ward, T.J., Woodward, D.E., van Mullem, J.A. (Eds.), 2009. Curve Number Hydrology: State of the Practice. ASCE, Reston, VA.
- He, M., Han, Q., 1982. Stochastic model of incipient sediment motion. Journal of the Hydraulics Division 108 (2), 211-224.
- Heckmann, T., Schwanghart, W., 2013. Geomorphic coupling and sediment connectivity in an alpine catchment—Exploring sediment cascades using graph theory.
- Geomorphology 182, 89-103. Hooke, J., 2003. Coarse sediment connectivity in river channel systems: a conceptual framework and methodology. Geomorphology 56 (1), 79-94.
- Hsu, S.M., Holly Jr, F.M., 1992. Conceptual bed-load transport model and verification for sediment mixtures. Journal of Hydraulic Engineering 118 (8), 1135-1152.
- Hupp, C.R., 2000. Hydrology, geomorphology and vegetation of Coastal Plain rivers in the south-eastern USA. Hydrol. Process. 14 (16–17), 2991–3010.
- Husic, A., Fox, J., Agouridis, C., Currens, J., Ford, W., Taylor, C., 2017a. Sediment carbon fate in phreatic karst (Part 1): Conceptual model development. J. Hydrol. 549, 179-193.
- Husic, A., Fox, J., Ford, W., Agouridis, C., Currens, J., Taylor, C., 2017b. Sediment carbon fate in phreatic karst (Part 2): Numerical model development and application. J. Hvdrol. 549, 208-219.
- Jaeger, K.L., Sutfin, N.A., Tooth, S., Michaelides, K., Singer, M., 2017. Geomorphology and Sediment Regimes of Intermittent Rivers and Ephemeral Streams. In: Intermittent Rivers and Ephemeral Streams, pp. 21-49.
- Jain, V., Tandon, S.K., 2010. Conceptual assessment of (dis) connectivity and its application to the Ganga River dispersal system. Geomorphology 118 (3), 349-358.
- Jain, S.C., 2001. Open-channel flow. John Wiley & Sons, pp. 58.

  Jarritt, N.P., Lawrence, D.S.L., 2007. Fine sediment delivery and transfer in lowland catchments: modelling suspended sediment concentrations in response to hydrological forcing. Hydrol. Process. 21 (20), 2729-2744.
- Jencso, K.G., McGlynn, B.L., Gooseff, M.N., Wondzell, S.M., Bencala, K.E., Marshall, L.A., 2009. Hydrologic connectivity between landscapes and streams: Transferring reachand plot-scale understanding to the catchment scale. Water Resour. Res. 45 (4).
- Jin, C.X., Dabney, S.M., Romkens, M.J.M., 2002. Trapped mulch increases sediment removal by vegetative filter strips: a flume study. Trans. ASAE 45, 929-939.
- Jin, C.X., Romkens, M.J.M., 2001. Experimental studies of factors in determining sediment trapping in vegetative filter strips. Trans. ASAE 44, 277-288.
- Kentucky Geologic Survey, 2017. Kentucky LiDAR sinkholes. Kentucky Geological Survey, University of Kentucky, KY USA.
- Knighton, A.D., 1989. River adjustment to changes in sediment load: the effects of tin mining on the Ringarooma River, Tasmania, 1875-1984. Earth Surf. Proc. Land. 14 (4), 333-359.
- Kronvang, B., Andersen, I.K., Hoffmann, C.C., Pedersen, M.L., Ovesen, N.B., Andersen, H.E., 2007. Water exchange and deposition of sediment and phosphorus during inundation of natural and restored lowland floodplains. Water Air Soil Pollut. 181 (1-4), 115-121.
- KYAPED, 2014. Kentucky Aerial Photography and Elevation Data Program. Accessed: 01/30/13. http://kygeonet.ky.gov/kyfromabove/.
- Lal, R., 1999. Soil management and restoration for C sequestration to mitigate the accelerated greenhouse effect. Progr. Environ. Sci. 1 (4), 307-326.
- Latocha, A., 2014. Geomorphic connectivity within abandoned small catchments (Stołowe Mts, SW Poland). Geomorphology 212, 4-15.
- Le Bissonnais, Y., Lecomte, V., Cerdan, O., 2004. Grass strip effects on runoff and soil loss. Agronomie 24, 129-136.
- Leopold, L.B., Wolman, M.G., Miller, J.P., 1964. Fluvial Processes in Geomorphology. W.H. Freeman, New York.
- Lewis, S.M., Barfield, B.J., Storm, D.E., Ormsbee, L.E., 1994. Proril—an erosion model using probability distributions for rill flow and density I. Model development. Transactions of the ASAE 37 (1), 115-123.
- Lexartza-Artza, I., Wainwright, J., 2009. Hydrological connectivity: linking concepts with

- practical implications. Catena 79 (2), 146-152.
- Lisle, I.G., Rose, C.W., Hogarth, W.L., Hairsine, P.B., Sander, G.C., Parlange, J.Y., 1998. Stochastic sediment transport in soil erosion. Journal of Hydrology 204 (1-4), 217-230.
- Liu, Y., Fu, B., 2016. Assessing sedimentological connectivity using WATEM/SEDEM model in a hilly and gully watershed of the Loess Plateau, China. Ecol. Indicators 66,
- Liu, X.M., Mang, X.Y., Zhang, M.H., 2008. Major factors influencing the efficacy of vegetated buffers on sediment trapping: A review and analysis. J. Environ. Qual. 37,
- López-Vicente, M., Sun, X., Onda, Y., Kato, H., Gomi, T., Hiraoka, M., 2017. Effect of tree thinning and skidding trails on hydrological connectivity in two Japanese forest catchments. Geomorphology 292, 104-114.
- Lumborg, U., 2004. Cohesive sediment transport modelling—application to the Lister Dyb tidal area in the Danish Wadden Sea. Journal of Coastal Research 114-123
- Mahoney, David Tyler, 2017. Sediment transport modelling using dynamic (dis)connectivity prediction for a bedrock controlled catchment. Theses and Dissertations-University of Kentucky Department of Civil Engineering. 55. https://uknowledge. ukv.edu/ce etds/55
- Maidment, D.R., 2002. Arc Hydro: GIS for water resources (Vol. 1). ESRI, Inc.
- Malmon, D.V., Dunne, T., Reneau, S.L., 2003. Stochastic theory of particle trajectories through alluvial valley floors. The Journal of Geology 111 (5), 525-542.
- Maner, Sam B., Barnes, L.H., 1953. Suggested criteria for estimating gross sheet erosion and sediment delivery rates for the blackland prairies problem area in soil conservation. U. S. Dept. Agr., Soil Cons. Serv., Fort Worth, pp. 17.
- Marchamalo, M., Hooke, J.M., Sandercock, P.J., 2016. Flow and Sediment Connectivity in Semi-arid Landscapes in SE Spain: Patterns and Controls. Land Degrad. Dev. 27 (4), 1032-1044.
- Masselink, R.J., Keesstra, S.D., Temme, A.J., Seeger, M., Giménez, R., Casalí, J., 2016. Modelling discharge and sediment yield at catchment scale using connectivity components. Land Degrad. Dev. 27 (4), 933-945.
- McGrain, P., 1983. The geologic story of Kentucky. Kentucky Geological Survey, University of Kentucky, Special Publication 8, Series XI.
- Meade, R.H., Yuzyk, T.R., Day, T.J., 1990. Movement and storage of sediment in rivers of the United States and Canada. In: Surface Water Hydrology. Geological Society of America, Boulder, Colorado, pp. 255-280, 21 fig, 3 tab, 185 ref.
- Merritt, W.S., Letcher, R.A., Jakeman, A.J., 2003, A review of erosion and sediment transport models. Environ. Modell. Software 18 (8), 761–799.
- Messenzehl, K., Hoffmann, T., Dikau, R., 2014, Sediment connectivity in the high-alpine valley of Val Müschauns, Swiss National Park—linking geomorphic field mapping with geomorphometric modelling. Geomorphology 221, 215-229.
- Michaelides, K., Wainwright, J., 2002. Modelling the effects of hillslope–channel coupling on catchment hydrological response. Earth Surf. Proc. Land. 27 (13), 1441–1457.
- Millar, R.G., Quick, M.C., 1998. Stable width and depth of gravel-bed rivers with cohesive banks. J. Hydraul. Eng. 124 (10), 1005-1013.
- Mockus, V., 1961. Watershed lag. U.S. Dept. of Agriculture, Soil Conservation Service, ES-1015, Washington, DC.
- Montgomery, D.R., Dietrich, W.E., 1994. Landscape dissection and drainage area-slope thresholds. In: Kirkby, M.J. (Ed.), Process Models and Theoretical Geomorphology. Wiley, Chichester, pp. 221-246.
- Moriasi, D.N., Arnold, J.G., Van Liew, M.W., Bingner, R.L., Harmel, R.D., Veith, T.L., 2007. Model evaluation guidelines for systematic quantification of accuracy in watershed simulations. Trans. ASABE 50 (3), 885-900.
- Morris, G.L., Fan, J., 2009. Reservoir Sedimentation Handbook. Design and Management of Dams, Reservoirs, and Watersheds for Sustainable Use. McGraw-Hill.
- Nachtergaele, J., Poesen, J., Sidorchuk, A., Torri, D., 2002. Prediction of concentrated flow width in ephemeral gully channels. Hydrol. Process. 16 (10), 1935-1953.
- Natural Resource Conservation Service NRCS, 1972. "Hydrology." National engineering handbook, Sec. 4, U.S. Department of Agriculture, Washington, D.C.
- Natural Resource Conservation Service NRCS, 2009. Web soil survey. URL http://www. websoilsurvey. ncsc. usda. gov/app/[verified October 29, 2009].
- Natural Resource Conservation Service NRCS, 2010. Time of Concentration. Part 630 Hydrology National Engineering Handbook. Accessed 5/4/2017.
- Neitsch, S.L., Arnold, J.G., Kiniry, J.R., Williams, J.R., 2011. Soil and water assessment tool theoretical documentation version 2009. Texas Water Resources Institute.
- Owens, P.N., Duzant, J.H., Deeks, L.K., Wood, G.A., Morgan, R.P.C., Collins, A.J., 2007. Evaluation of contrasting buffer features within an agricultural landscape for reducing sediment and sediment-associated phosphorus delivery to surface waters. Soil Use Manag. 23, 165-175.
- Palanisamy, B., Workman, S.R., 2014. Hydrologic modeling of flow through sinkholes located in streambeds of Cane Run Stream, Kentucky. J. Hydrol. Eng. 20 (5), 04014066
- Pan, C., Huang, W., 2010. Journal of Coastal Research. Numerical modeling of suspended sediment transport affected by tidal bore in Qiantang Estuary 26 (6), 1123-1132.
- Papanicolaou, A.N., Diplas, P., Evaggelopoulos, N., Fotopoulos, S., 2002. Stochastic incipient motion criterion for spheres under various bed packing conditions. Journal of Hydraulic Engineering 128 (4), 369-380.
- Partheniades, E., 1965. Erosion and deposition of cohesive soils. J. Hydraul. Div. 91 (1), 105-139.
- Phillips, J.D., 2003. Sources of nonlinearity and complexity in geomorphic systems. Prog. Phys. Geogr. 27 (1), 1-23.
- Phillips, J.D., 2015. Badass geomorphology. Earth Surf. Proc. Land. 40, 22-33.
- Phillips, J.D., Martin, L.L., Nordberg, V.G., Andrews, W.A., 2004. Divergent evolution in fluviokarsts landscapes of Central Kentucky. Earth Surf. Proc. Land. 29, 799-819.
- Phillips, J.D., Šamonil, P., Pawlik, Ł., Trochta, J., Daněk, P., 2017. Domination of hillslope denudation by tree uprooting in an old-growth forest. Geomorphology 276, 27-36.

- Pringle, C., 2003. What is hydrologic connectivity and why is it ecologically important? Hydrol. Process. 17 (13), 2685–2689.
- Quinton, J.N., 1997. Reducing predictive uncertainty in model simulations: a comparison of two methods using the European Soil Erosion Model (EUROSEM). Catena 30 (2–3), 101–117.
- Radbruch-Hall, D.H., Colton, R.B., Davies, W.E., Lucchitta, I., Skipp, B.A., Varnes, D.J., 1982. Digital Compilation of Landslide Overview Map of the Conterminous United States, United States Geological Survey Professional Paper 1183. Government Printing Office, Washington D.C, U.S.
- Reed, T.M., McFarland, J.T., Fryar, A.E., Fogle, A.W., Taraba, J.L., 2010. Sediment discharges during storm flow from proximal urban and rural karst springs, central Kentucky, USA. J. Hydrol. 383 (3–4), 280–290.
- Rienzi, E.A., Fox, J.F., Grove, J.H., Matocha, C.J., 2018. Experimental results and temporal surrogate modeling of particulate organic carbon released during interrill erosion. CATENA 163, 1–12.
- Roberts, R.G., Church, M., 1986. The sediment budget in severely disturbed watersheds, Queen Charlotte Ranges, British Columbia. Can. J. For. Res. 16 (5), 1092–1106.
- Robichaud, P.R., Elliot, W.J., Pierson, F.B., Hall, D.E., Moffet, C.A., 2007. Predicting postfire erosion and mitigation effectiveness with a web-based probabilistic erosion model. Catena 71 (2), 229–241.
- Roehl, J.W., 1962. Sediment source areas, delivery ratios and influencing morphological factors. Int. Assoc. Sci. Hydrol. 59, 202–213.
- Roering, J.J., Kirchner, J.W., Dietrich, W.E., 1999. Evidence for nonlinear, diffusive sediment transport on hillslopes and implications for landscape morphology. Water Resour. Res. 35 (3), 853–870.
- Rosgen, D.L., (2001, March). A practical method of computing streambank erosion rate. In: Proceedings of the Seventh Federal Interagency Sedimentation Conference (Vol. 1).
- Russo, J., Fox, J., 2012. The Role of the Surface Fine-Grained Laminae in Low-Gradient Streams: A Model Appraoch. Geomorphology 171–172.
- Russo, Joseph Paul, 2000. Investigation of surface fine grained laminae, streambed, and streambank processes using a watershed scale hydrologic and sediment transport model. University of Kentucky Doctoral Dissertations, p. 750.
- Schumm, Stanley A., 1954. The relation of drainage basin relief to sediment loss. Int. Assn. Hydrol. IUGG Tenth Gen. Assembly Rome 1, 216–219.
- Schumm, S.A., 1977. The fluvial system, pp. 338. New York, NY: Willey.
- Seaber, P.R., Kapinos, F.P., and Knapp, G.L. (1987). Hydrologic Unit Maps: U.S. Geological Survey Water-Supply Paper 2294, 63 p.
- Sims, R.P., Preston, D.G., Richardon, A.J., Newton, J.H., Isgrig, D., Blevins, R.L., 1968.
  Soil survey of Fayette county, Kentucky. USDA Soil Conservation Service, U.S.
  Government Printing Office, Washington D.C.
- Smallwood, R., 2017. Personal Communication. February 16, 2017.
- USDA Soil Science Division Staff, 2017. Soil survey manual. In: Ditzler, C., Scheffe, K., Monger, H.C. (eds.). USDA Handbook 18. Government Printing Office, Washington, D.C.
- Souza, J.O., Correa, A.C., Brierley, G.J., 2016. An approach to assess the impact of landscape connectivity and effective catchment area upon bedload sediment flux in Saco Creek Watershed, Semigrid Brazil, Catena 138, 13–29.
- SWAT, 2012. SWAT: Model use, calibration, and validation. Trans. ASABE 55 (4), 1491–1508.
- Taylor, C.J., 1992. Ground-water Occurrence and Movement Associated with Sinkhole Alignments in the Inner Bluegrass Karst Region of central Kentucky MS Thesis. University of Kentucky, Lexington, Kentucky.
- Taylor, C.J., Nelson, H.L., 2008. A compilation of provisional karst geospatial data for the

- Interior Low Plateaus physiographic region, central United States (No. 339). Geological Survey (US).
- Taylor, P.D., Fahrig, L., Henein, K., Merriam, G., 1993. Connectivity is a vital element of landscape structure. Oikos 571–573.
- Tazioli, G.S., 1981. Nuclear techniques for measuring sediment transport in natural stream – examples from instrumented basins. Int. Assoc. Hydrol. Sci. Publ. 133, 63-68
- Third Rock Consulting, 2016. LFUCG Stormwater Stakeholder Advisory Committee.

  Accessed 2/18/2016. http://www.lexingtonky.gov/Modules/ShowDocument.as-px?documentid = 27603
- Thrailkill, J., 1974. Pipe flow models of a Kentucky limestone aquifer. Groundwater 12 (4), 202–205.
- Thrailkill, J., Sullivan, S.B., Gouzie, D.R., 1991. Flow parameters in a shallow conduit flow carbonate aquifer, Inner Bluegrass Karst Region, Kentucky, USA. J. Hydrol. 129 (1) 87–108
- Tisdall, J.M., Oades, J., 1982. Organic matter and water-stable aggregates in soils. J. Soil Sci. 33 (2), 141–163.
- Torri, D., Poesen, J., 2014. A review of topographic threshold conditions for gully head development in different environments. Earth Sci. Rev. 130, 73–85.
- Torri, D., Biancalani, R., Poesen, J., 1990. Initiation of motion of gravels in concentrated overland flow: cohesive forces and probability of entrainment. Catena, Supplement 17, 79–90
- Trimble, S.W., 1993. The distributed sediment budget model and watershed management in the Paleozoic plateau of the upper midwestern United States. Phys. Geogr. 14, 285–303
- Ulack, R., Raitz, K., Pauer, G., 1998. Atlas of Kentucky: Lexington, University Press of USEPA (United States Environmental Protection Agency), Office of Science and Technology, 1999. Protocol for Developing Sediment TMDLs. EPA 841-B-99-004. Office of Water (4503F), United States Environmental Protection Agency, Washington D.C., p. 132.
- USEPA, 2004. The Incidence and Severity of Sediment Contamination in Surface Waters of the United States, EPA 823-R-04-007. http://www.epa.gov/waterscience/cs/report/2004/nsqs2ed-complete.pdf
- Vandaele, K., Poesen, J., Govers, G., vanWesemael, B., 1996. Geomorphic threshold conditions for ephemeral gully incision. Geomorphology 16, 161–173.
- Vandaele, K., 1993. Assessment of factors affecting ephemeral gully erosion in cultivated catchments of the Belgian Loam Belt. In: S. Wicherek (Editor), Farm Land Erosion in Temperate.
- Verhoff, F.H., Melfi, D.A., Yaksich, S.M., 1979. Storm travel distance calculations for total phosphorus and suspended materials in rivers. Water Resour. Res. 15, 1354–1360.
- phosphorus and suspended materials in rivers. Water Resour. Res. 15, 1354–1360 Walling, D.E., 1983. The sediment delivery problem. J. Hydrol. 65 (1–3), 209–237.
- Walling, D.E., Collins, A.L., Jones, P.A., Leeks, G.J.L., Old, G., 2006. Establishing fine-grained sediment budgets for the Pang and Lambourn LOCAR catchments, UK. J. Hydrol. 330 (1), 126–141.
- Wanielista, M., Kersten, R., Eaglin, R., 1997. Hydrology: water quantity and quality control. John Wiley and Sons.
- Wright, A.C., Webster, R., 1991. A stochastic distributed model of soil erosion by overland flow. Earth Surface Processes and Landforms 16 (3), 207–226.
- Wu, F.C., Chou, Y.J., 2003. Rolling and lifting probabilities for sediment entrainment. Journal of Hydraulic Engineering 129 (2), 110–119.
- Zhu, J., Taylor, T.P., Currens, J.C., Crawford, M.M., 2014. Improved karst sinkhole mapping in Kentucky using LIDAR techniques: a pilot study in Floyds Fork Watershed. J. Cave Karst Stud. 76 (3), 207.